

1 **RESEARCH ARTICLE**

2
3 **Establishing *Physalis* as a *Solanaceae* model system enables genetic**
4 **reevaluation of the inflated calyx syndrome**

5
6 **Jia He^{1,2}, Michael Alonge^{3†}, Srividya Ramakrishnan³, Matthias Benoit^{1,2†}, Sebastian Soyk^{1,†}, Nathan**
7 **T. Reem^{4†}, Anat Hendelman¹, Joyce Van Eck^{4,5}, Michael C. Schatz^{1,3,6}, Zachary B. Lippman^{1,2,*}**

8
9 ¹ Cold Spring Harbor Laboratory, Cold Spring Harbor, NY 11724, USA

10 ² Howard Hughes Medical Institute, Cold Spring Harbor Laboratory, Cold Spring Harbor, NY 11724,
11 USA

12 ³ Department of Computer Science, Johns Hopkins University, Baltimore, MD 21218, USA

13 ⁴ Boyce Thompson Institute, Ithaca, NY 14853, USA

14 ⁵ Plant Breeding and Genetics Section, School of Integrative Plant Science, Cornell University, Ithaca,
15 NY 14853, USA

16 ⁶ Department of Biology, Johns Hopkins University, Baltimore, MD 21218, USA

17 [†] Current addresses: Ohalo Genetics, Aptos, CA 95003, USA (M.A.); LIPME, Université de Toulouse,
18 INRAE, CNRS, Castanet-Tolosan 31326, France (M.B.); Center for Integrative Genomics, University of
19 Lausanne, CH-1005 Lausanne, Switzerland (S.S.); Benson Hill, St. Louis MO 63132 (N.T.R).

20 * To whom correspondence may be addressed:
21 lippman@cshl.edu

22
23 The author responsible for distribution of materials integral to the findings presented in this article in
24 accordance with the policy described in the Instructions for Authors (<https://academic.oup.com/plcell>) is:
25 Zachary B. Lippman (lippman@cshl.edu).

26
27 **ABSTRACT**

28 The highly diverse *Solanaceae* family contains several widely studied model and crop species. Fully
29 exploring, appreciating, and exploiting this diversity requires additional model systems. Particularly
30 promising are orphan fruit crops in the genus *Physalis*, which occupy a key evolutionary position in the
31 *Solanaceae* and capture understudied variation in traits such as inflorescence complexity, fruit ripening
32 and metabolites, disease and insect resistance, self-compatibility, and most notable, the striking inflated
33 calyx syndrome (ICS), an evolutionary novelty found across angiosperms where sepals grow
34 exceptionally large to encapsulate fruits in a protective husk. We recently developed transformation and
35 genome editing in *Physalis grisea* (groundcherry). However, to systematically explore and unlock the
36 potential of this and related *Physalis* as genetic systems, high-quality genome assemblies are needed.
37 Here, we present chromosome-scale references for *P. grisea* and its close relative *P. pruinosa* and use
38 these resources to study natural and engineered variation in floral traits. We first rapidly identified a
39 natural structural variant in a *bHLH* gene that causes petal color variation. Further, and against
40 expectations, we found that CRISPR-Cas9 targeted mutagenesis of 11 MADS-box genes, including
41 purported essential regulators of ICS, had no effect on inflation. In a forward genetics screen, we
42 identified *huskless*, which lacks ICS due to mutation of an *AP2-like* gene that causes sepals and petals to

merge into a single whorl of mixed identity. These resources and findings elevate *Physalis* to a new *Solanaceae* model system, and establish a paradigm in the search for factors driving ICS.

INTRODUCTION

The *Solanaceae* family is one of the most important plant families in fundamental and applied research due not only to its remarkable morphological and ecological diversity but also to its far-reaching economic value from its many members used as food crops, ornamentals, and sources of pharmaceuticals (Añibarro-Ortega et al., 2022; Gebhardt, 2016; Shenstone et al., 2020). The most studied *Solanaceae* include major food crops such as eggplant (*Solanum melongena*), pepper (*Capsicum annuum*), potato (*Solanum tuberosum*), and tomato (*Solanum lycopersicum*), in addition to the model species petunia (*Petunia hybrida*) and *Nicotiana benthamiana*. However, various species-specific limitations of the other taxa have made tomato a preferred model for many studies, as it has a full suite of genetic and genomic resources that enable maximal biological discovery and translation to agriculture.

Developing new *Solanaceae* model systems that equal the utility of tomato is essential to study incompletely explored diversity, including traits of economic importance. Most challenging is identifying potential systems with noteworthy comparative and species-specific variation that, critically, can be dissected by efficient forward and reverse genetics that is enabled by tractable genomics, genome editing, and cultivation. We previously identified species in the genus *Physalis* as promising in all these aspects (Lemmon et al., 2018). This genus includes orphan crops such as tomatillo (*P. philadelphica* and *P. ixocarpa*), goldenberry (*P. peruviana*), and groundcherry (*P. grisea* and *P. pruinosa*), and many other species that yield edible fruits or are grown as ornamentals.

Physalis occupies a key phylogenetic position that complements other *Solanaceae* models. It is a representative genus of Physaleae, an under-studied *Solanaceae* tribe that has the most genera in the family (Deanna et al., 2019; Pretz & Deanna, 2020; Zamora-Tavares et al., 2016), and diverged from established *Solanum* model systems about 19 million years ago (Ma) (Särkinen et al., 2013). In addition, recently discovered Physaloid fruiting fossils dated to about 52 Ma pushed back the evolutionary timing of *Solanaceae* divergence from other taxa considerably (Deanna et al., 2020; Wilf et al., 2017). Thus, *Physalis* has great potential to analyze diversification over long evolutionary distances in comparative studies within the *Solanaceae*. Moreover, *Physalis* species show substantial variation in developmental and

molecular traits, including inflorescence complexity, secondary metabolism, and disease resistance (Baumann & Meier, 1993; Huang et al., 2020; Park et al., 2014; Whitson, 2012; W.-N. Zhang & Tong, 2016), providing additional avenues for discovery. However, the most conspicuous and impressive feature of *Physalis*, also found in other angiosperms, is the inflated calyx syndrome (ICS), a remarkable evolutionary novelty where sepals grow excessively large after fertilization to form balloon-like husks that encapsulate fruits (He et al., 2004; Wilf et al., 2017).

Dissecting the evolutionary and mechanistic origins of morphological novelties is a fundamental goal in biology (Muller & Wagner, 1991; Shubin et al., 2009), and it is not surprising that botanists and evolutionary biologists have long been fascinated by ICS (He et al., 2004; U. T. Waterfall, 1958; Wilf et al., 2017). Though *Physalis* has historically lacked molecular and functional genetics tools, studies on ICS over the last few decades have suggested a central role for two MADS-box genes, including an ortholog of one gene in potato, *StMADS16* (an ortholog of *Arabidopsis thaliana* *AGAMOUS-LIKE 24*), which causes leaf-like sepals when overexpressed in other *Solanaceae* (He et al., 2004). Prompted by this observation, supportive molecular and functional genetic data generated within *Physalis* suggested that heterotopic expression of the *StMADS16* ortholog *MPF2* was key to the evolution of ICS. Later studies suggested this essential role emerged from modified *cis*-regulatory control of *MPF2* by the *euAPI*-like gene *MPF3* (He & Saedler, 2005; Zhao et al., 2013).

A recent genome of *P. floridana* and additional functional work suggested that loss of another MADS-box gene, *MBP21/JOINTLESS-2 (J2)*, a member of the *SEPALLATA4 (SEP4)* clade, was also critical, and seemingly reinforced an additional conclusion that fertilization is an integral physiological driver of ICS (Lu et al., 2021). The proposed role of fertility and previous findings that flower-specific *MPF2* expression is ancestral to ICS suggested this trait may have been lost during evolution (He & Saedler, 2007; Hu & Saedler, 2007). However, a recent deeply sampled taxonomic study showed that, although being invariantly present in a large monophyletic clade such as *Physalis* subgenus *Rydbergi*, ICS was gained multiple times throughout the tribe of Physalideae in a stepwise and directional manner, from noninflation to enlarged sepals appressed to the fruit (accrescent-appressed), and finally to an inflated calyx (Deanna et al., 2019). These findings, along with independent emergence of ICS in other angiosperms (Deanna et al., 2019), may indicate that there is a deeper genetic and molecular

complexity behind ICS, determined by factors besides *MPF2* and other proposed *MADS-box* genes (Deanna et al., 2019; Hu & Saedler, 2007).

Outstanding questions regarding ICS and our broad interest in *Solanaceae* biology and agriculture led us several years ago to begin establishing *Physalis* as a new model system. We developed efficient *Agrobacterium*-mediated transformation and CRISPR-Cas9 genome editing in the diploid groundcherry species *P. grisea*, and demonstrated the utility of these tools by mutating orthologs of tomato domestication genes in groundcherry to improve productivity traits (Lemmon et al., 2018; Swartwood & Van Eck, 2019). More recently, *P. grisea* was critical in revealing pleiotropic functions of an ancient homeobox gene, and in dissecting the evolution of redundancy between duplicated signaling peptide genes controlling stem cell proliferation in the *Solanaceae* (Hendelman et al., 2021; Kwon et al., 2022). However, high-quality reference genomes of *P. grisea* and other species have been lacking, and are needed to promote the full potential and deployment of this system as has been achieved in tomato. Here, we report high-quality chromosome-scale genomes for *P. grisea* and its close relative *P. pruinosa*. We demonstrate the power of these resources in enabling forward and reverse genetics by revealing multiple genotype-to-phenotype relationships in floral development, including ICS. Our work establishes *Physalis* as a new *Solanaceae* reference system that can advance comprehensive studies of long-standing and emerging biological questions within and beyond the genus.

RESULTS

Chromosome-scale reference genomes of *P. grisea* and *P. pruinosa*

Among *Solanaceae* genera, *Physalis* is more closely related to *Capsicum* (pepper) than *Solanum* (eggplant, potato, tomato) (**Figure 1A**). Chinese lantern (*Alkekengi officinarum*, closely related to *Physalis*), tomatillo (*Physalis philadelphica* and *Physalis ixocarpa*) and many other *Physalis* orphan crops are self-incompatible, large plants with tetraploid genomes, making them challenging to develop into model systems. In contrast, the groundcherry species *P. grisea*, *P. pruinosa*, and close relatives have reasonable genome sizes (estimated ~1-2 Gb), are diploid, self- and cross-compatible, have rapid generation times (first mature fruit 66-70 days after sowing), and are easy to grow and manage in both greenhouses and fields. The taxonomy and naming of *Physalis* species has a convoluted past that was recently clarified (Pretz & Deanna, 2020). *P. pruinosa* was initially designated to describe *Physalis* in the northeastern United States,

showing erect or prostrate growth with large, thick and coarsely sinuate-dentate leaves (Rydberg, 1896). A revision of *Physalis* in the last century proposed *P. pubescens* var. *grisea* to differentiate species included in *P. pruinosa* (U. T. Waterfall, 1958). Additional species were then identified (U. T. Waterfall, 1967), and *P. pubescens* var. *grisea* was ultimately recognized as a separate species, *P. grisea* (Martínez, 1993; Pretz & Deanna, 2020).

As *P. grisea* and *P. pruinosa* are closely related, they share similar vegetative and reproductive shoot and organ morphologies, including inflated calyxes encapsulating fruits of similar size, shape, and color (**Figure 1B-D**). Their primary shoots terminate in a single flower inflorescence after 5-6 leaves, and new shoots emerge according to the sympodial growth habit that is characteristic of all *Solanaceae* (Lemmon et al., 2018). In *Physalis*, sympodial units comprise one leaf, one flower and two axillary (sympodial) shoots (**Figure 1C**). A conspicuous feature distinguishing *P. pruinosa* from *P. grisea* is the absence of purple pigmentation on stems and petal nectar guides. *P. pruinosa* also has narrower leaves and a smaller stature due to shorter internodes (**Figure 1B, D; Supplemental Data Set S1**).

Based on the features described, *P. grisea* and *P. pruinosa* are excellent candidates occupying a key phylogenetic position among *Solanaceae* model systems. We integrated PacBio high fidelity (HiFi) and Oxford Nanopore (ONT) long-read sequencing to establish highly accurate and complete chromosome-scale genome assemblies for both species, with assembly sizes of 1.37 Gb for *P. grisea* and 1.38 Gb for *P. pruinosa* (**Figure 1E**). The *P. grisea* and *P. pruinosa* assemblies are the first *Physalis* genus reference-quality assemblies, demonstrating substantially improved contiguity, accuracy, and completeness compared to a recent *P. floridana* genome (Lu et al., 2021) (**Supplemental Table S1**). Specifically, the *P. floridana* genome has an error rate (errors/bp) of 3.83×10^{-4} and a contig N50 of 4.6 Mbp, whereas our assemblies produced substantially lower error rates of 3.09×10^{-6} (*P. grisea*) and 1.66×10^{-6} (*P. pruinosa*) and much higher contig N50s of 31.6 and 82.2 Mbp, respectively, with gapless assemblies of chromosomes 5 and 7 for *P. pruinosa*.

Based on RNA-sequencing data from vegetative and reproductive tissues ((Lemmon et al., 2018), and **Methods**), we annotated 33,833 and 34,187 genes in the *P. grisea* and *P. pruinosa* assemblies, respectively (**Supplemental Table S2**), with most genes concentrated at the ends of the 12 chromosomes, as was observed in other *Solanaceae* genomes (Kim et al., 2014; Sato et al., 2012; Wei et al., 2020; X. Xu et al., 2011) (**Figure 1E**, see **Methods**). Both

genomes are highly repetitive, with 79% of the sequence representing transposable elements, especially LTR retrotransposons (**Figure 1E**). Comparing the two genomes, we observed nearly complete macrosynteny across all 12 chromosomes, consistent with the close relationship of these species, but also detected a few small-scale inversions and translocations (**Figure 1E**). Calling single nucleotide polymorphisms (SNPs) using *P. pruinosa* Illumina short read sequences against the *P. grisea* reference revealed 60,087 homozygous SNPs, with predicted high impact changes (SNPeff, (Cingolani et al., 2012)) on 43 gene transcripts (**Supplemental Table S3, S4**). Despite the broad similarity of these genomes, we identified over 900 structural variants (SVs) between 30 bp and 10 kbp in length, many of which intersect coding and putative *cis*-regulatory sequences (**Figure 1F, G and Supplemental Table S5, Supplemental Data Set S2**). Some of these variants could explain phenotypic differences between *P. grisea* and *P. pruinosa*.

A structural variant in the bHLH transcription factor gene *ANTHOCYANIN1* controls nectar guide color variation

We first sought to utilize our genomes to map the most conspicuous phenotype distinguishing the two species, nectar guide color variation. *P. grisea* displays deep purple nectar guides typical of most *Physalis* species, whereas *P. pruinosa* does not. (**Figure 2A**). This pigmentation difference is also found on stems and branches. Crossing *P. grisea* and *P. pruinosa* resulted in F1 hybrids showing purple pigmentation, and an F2 population showed that the yellow color segregated as a single recessive mutation. Mapping-by-sequencing localized the mutation to chromosome 4; however, limited recombination resulted in a large interval spanning most of the chromosome (**Figure 2B**).

To identify candidate genes, we searched for homologs of genes involved in the production of anthocyanins in the *Solanaceae* genus *Petunia*. Anthocyanins belong to a class of polyphenolic secondary metabolites named flavonoids, and one outcome of their accumulation in tissues and organs is purple pigmentation (Liu et al., 2018). Many ornamental *Petunia* species show variation in anthocyanin accumulation, and studies on this diversity have identified enzymes and transcription factors in the anthocyanin pathway (Bombarely et al., 2016; Liu et al., 2018).

Anthocyanin biosynthesis involves three major steps, including the conversion of phenylalanine to 4-coumaroyl-CoA through stepwise enzymatic reactions, and the conversion of 4-coumaroyl-CoA to dihydroflavonols, which are precursors in the final synthesis steps of specific anthocyanins (**Figure 2C**). We identified four orthologs of anthocyanin pathway genes and their regulators on chromosome 4. Overlaying our SV analysis revealed a mutation in only one of these genes, a 43 bp deletion in the second intron of the *P. pruinosa* gene Phypru04g010390, which encodes a bHLH transcription factor orthologue of petunia ANTHOCYANIN1 (AN1) (Spelt et al., 2000) (**Figure 2D**). AN1 activates the structural gene *DIHYDROFLAVONOL REDUCTASE* and other anthocyanin regulators (Spelt et al., 2000). Notably, mutations in petunia *ANI* result in loss of anthocyanins in all tissues (Spelt et al., 2000, 2002). Using RT-PCR and sequencing of cDNA, we found that *ANI* transcripts in *P. pruinosa* were longer than those in *P. grisea* due to a retention of 179 bp from intron 2, which results in a premature stop codon (**Figure 2E**). We validated this result by CRISPR-Cas9 targeting *PgANI* (Phygri04g010290) in *P. grisea*. Five out of 11 first generation (T₀) transgenic lines failed to produce anthocyanins, and sequencing showed that these plants carried edited alleles of *PgANI* (**Figure 2F, G**). Though another variant closely linked to *ANI* on chromosome 4 could be responsible for the color variation, our genetic and molecular results strongly support that the SV in *P. pruinosa ANI* (*PprANI*) underlies the absence of purple pigmentation in *P. pruinosa* and further demonstrate the utility of our genomic resources in deploying forward genetics in *Physalis*.

The MADS-box genes *MPF2* and *MPF3* are not essential regulators of ICS.

The most striking feature of *Physalis* is the ICS, which evolved repeatedly in other *Solanaceae* genera and angiosperms (Deanna et al., 2019; Padmaja et al., 2014; Paton, 1990). Soon after fertilization, sepals undergo remarkable growth and expansion acropetally to encapsulate fruits in balloon-like papery husks, which may provide protection from pathogens and promote seed dispersal (**Figure 3A**) (Baumann & Meier, 1993; J. Li et al., 2019). Despite long-standing interest, the evolutionary and mechanistic origins of ICS remain unclear. One early defining study proposed that heterotopic expression of *MPF2* was essential to the evolution of ICS (He & Saedler, 2005). This hypothesis was based on overexpression of the potato ortholog *StMADS16* in tobacco (*Nicotiana tabacum*), which produced leaf-like sepals. Empirical support

in *Physalis* came from RNA interference (RNAi) knock-down of *MPF2* in *P. floridana*, where multiple transgenic lines showed a reduced calyx size, the severity of which was highly correlated with impaired fertility, but counterintuitively not the level of reduction of *MPF2* transcripts (He & Saedler, 2005).

Despite this contradictory result, follow-up studies proposed and tested an extended mechanism involving regulation of *MPF2* by the *API*-like transcription factor gene *MPF3* (orthologue of Arabidopsis *APETALA1* and tomato *MACROCALYX*), in combination with hormonal control and fertilization (He & Saedler, 2007; Zhao et al., 2013). However, functional data supporting these conclusions were based on overexpression, plus also RNAi and virus induced gene silencing (VIGS) knockdown of expression. Pleiotropic phenotypic outcomes are common in overexpression experiments, and are challenging to relate to specific genes studied, whereas RNAi and VIGS are difficult to interpret due to variable knock-down efficiencies and potential off-target effects (Senthil-Kumar & Mysore, 2011; P. Xu et al., 2006). Further convolution of a possible ICS mechanism emerged with the recent publication of the *P. floridana* genome, and the suggestion that absence of the *SEP4* orthologue of the tomato MADS-box gene *SIMBP21/J2* in *Physalis* was yet another critical factor in the origin of ICS (Lu et al., 2021).

To address these inconsistencies and provide a more robust genetic dissection of ICS, we first used CRISPR-Cas9 genome editing to eliminate *MPF2* and *MPF3* function in *P. grisea*. We generated five alleles of *PgMPF2* (Phygri11g023460) and four alleles of *PgMPF3* (Phygri12g018350) (**Figure 3B**), and these independent mutations caused different premature stop codons. Notably, none of these homozygous mutants disrupted ICS; all *Pgmpf2*^{CR} mutants showed similar calyx inflation as wild type (WT), and *Pgmpf3*^{CR} mutants displayed enlarged and more leaf-like tips of sepals before inflation, a phenotype also observed in tomato *mc* mutants (**Figure 3C**) (Yuste-Lisbona et al., 2016). Although this change of sepal tips was accompanied by a lower calyx height/width ratio (**Figure 3G**), inflation was unaffected. Besides the sepal phenotype, *Pgmpf3* also displayed abnormal branching patterns; *Pgmpf3* mutants frequently produced three instead of two sympodial shoots (**Figure 3D-F**). Finally, we generated double mutants to test whether eliminating *PgMPF2* and *PgMPF3* functions together would disrupt inflation. Notably, *Pgmpf2 Pgmpf3* plants matched the phenotypes of *Pgmpf3* single mutants, including the progression of ICS (**Figure 3H**). In summary, these CRISPR-Cas9 engineered loss-of-function mutations in *PgMPF2* and *PgMPF3* show that these MADS-box genes are not

responsible for the evolution of ICS and are not essential regulators of this developmental process.

Targeted mutagenesis of additional MADS-box genes does not abolish ICS.

In an effort to identify genes involved in ICS, we embarked on a more comprehensive reverse genetics approach targeting MADS-box genes known to regulate floral organ development in tomato and other species, including additional MADS-box family members that mimic ICS when overexpressed or mutated in non-ICS *Solanaceae*. For example, we characterized a spontaneous tomato mutant with greatly enlarged fleshy fruit-covering sepals and found a transposon insertion SV upstream of *TOMATO AGAMOUS-LIKE1 (TAGL1)* that caused >80-fold overexpression in developing sepals (**Figure 4A**). *TAGL1* belongs to the *AGAMOUS* clade of MADS-box transcription factors, and is a close paralog of *TOMATO AGAMOUS 1 (TAG1)*. Previous studies showed that both of these genes control flower development, and when either is overexpressed, enlarged and fleshy sepals are produced, in part mimicking ICS (Itkin et al., 2009; Pnueli et al., 1994). To test the roles of the *Physalis* orthologues of these genes, we generated CRISPR mutants. As observed in corresponding mutants of other species (Pan et al., 2010; Yanofsky et al., 1990), *Pgtagl^{CR-1}* homozygous mutants displayed severe homeotic transformation of stamens to petal-like structures, while *Pgtagl^{CR-1}* displayed similar but weaker homeotic transformations (**Figure 4B**). Importantly, despite these floral organ defects, accompanied also by partial or complete loss of self-fertilization, both of these mutants maintained inflation, although calyx size was reduced, potentially due to secondary growth effects (**Figure 4B-E**).

Based on their roles in floral organ development and inflorescence architecture, *SEPALLATA4 (SEP4)* MADS-box genes are another set of ICS candidates. Tomato has four *SEP4* clade MADS-box genes: *J2*, *SIMADSI/ENHANCER OF J2* (hereafter *EJ2*), *LONG INFLORESCENCE (LIN)* and *RIPENING INHIBITOR (RIN)*. We previously showed that *EJ2* and *LIN* regulate sepal development; mutants of *ej2* alone and in combination with *lin* develop enlarged sepals (Soyk et al., 2017). Analysis of the genome of *P. floridana* (Lu et al., 2021), and confirmed in our genomes, showed that *Physalis* lost the ortholog of *J2*, whereas the other three *SEP4* genes are present. Curiously, loss of *J2* was proposed to have promoted the evolution of ICS, but non-ICS *Solanaceae* such as pepper also lack *J2*. To test roles of the *SEP4* clade in ICS,

we used CRISPR-Cas9 to mutate all three *SEP4* genes in *P. grisea*. Notably, multiple independent mutations in *PgEJ2*, *PgLIN*, and *PgRIN* did not inhibit ICS. Similar to our findings in tomato *ej2* mutants (Soyk et al., 2017), mutants of *Pgej2^{CR-1}* produced larger sepals in young and fully developed flowers, but inflation proceeded normally, with the only modification being sepal tips failing to coalesce to a single point after inflation is complete (**Figure 4C**).

Fertilization is not required for ICS.

In flower development, B-class MADS-box genes participate in specifying petal and stamen identity, and the loss of B function leads to homeotic transformations of petals and stamens, which impaired self-fertilization (Theißen & Saedler, 2001; Weigel & Meyerowitz, 1994; Yanofsky et al., 1990). If fertilization-related signals were required for ICS, as reported (He & Saedler, 2007), mutations in B-class MADS-box genes should result in abnormal ICS development. Previously, a mutation deleting the B-class MADS-box gene *GLOBOSA1* (*GLO1*) was shown to develop a double-layered calyx phenotype in *P. floridana* when fertilized with WT pollen (J.-S. Zhang et al., 2014). We identified four B-class MADS-box genes in *P. grisea*, including the four closest homologs of *GLO1*: *PgGLO1* (Phygri01g009190), *PgGLO2* (Phygri06g017940), *PgDEF* (Phygri11g018450) and *PgTM6* (Phygri02g012900). CRISPR-Cas9 induced null mutations in all four genes failed to disrupt ICS. Mutants of *Pgtm6^{CR-1}* and *Pgglo2^{CR-1}* appeared WT, whereas *Pgglo1^{CR-1}* and *Pgdef^{CR-1}* both displayed expected homeotic transformations of stamens to carpels, and petals to sepals. Notably, calyx inflation was unaffected even in the second whorls of *Pgglo1^{CR-1}* and *Pgdef^{CR-1}* where petals were converted to sepals (**Figure 4D, E**).

Fertility or signals from developing fruits have also been observed to be required for the initiation and progression of inflation, perhaps due to the activity and signaling of hormones such as cytokinin and gibberellin (He & Saedler, 2007). However, many of our MADS-box mutants with severe floral organ homeotic transformations also fail to self-fertilize, and have various degrees of defects in fruit development. That ICS is unaffected in these mutants provides compelling genetic evidence that ICS can be uncoupled from normal fertilization. In particular, both *Pgdef^{CR-1}* and *Pgglo1^{CR-1}* homozygous mutants cannot self-fertilize and form multiple small fruits without seeds due to homeotic transformations of stamens to carpels, yet the twin outer layers of sepals still form inflated calyces (**Figure 4E**). Moreover, in *Pgtagl1^{CR-1}* and *Pgtagl^{CR-}*

^lmutants, which cannot self-fertilize and whose fruits arrest early in development or fail to form entirely, respectively, inflation remained intact (**Figure 4E**).

In summary, although earlier observations, hypotheses, and data suggested critical roles of several MADS-box genes in the evolution of ICS, our results show that calyx inflation is maintained in loss-of-function mutants of the *P. grisea* *AG* clade, *SEP4* clade and B-class MADS-box transcription factor genes. These data further demonstrate that although fertilization signals or developing fruit may contribute to the regulation of calyx inflation, neither is absolutely required.

The *huskless* mutant, caused by a mutation in an *AP2*-like transcription factor, eliminates inflated calyx

Forward genetics is a powerful and unbiased approach to identify genes controlling traits of interest in model systems. We performed a small-scale ethyl methanesulfonate (EMS) mutagenesis screen in *P. grisea* to identify genes involved in calyx development (**see Methods**). A recessive mutant bearing fruits without husks was identified and named *huskless* (*hu*) (**Figure 5A, B**). Scanning electron microscope (SEM) imaging of dissected flower buds showed that *hu* mutants developed three floral whorls instead of four compared to WT (**Figure 5C, D**). To isolate the causative mutation, we sequenced genomic DNA from a pool of *hu* mutants and WT siblings from the original *P. grisea* mutagenesis (M2) family (**see Methods**). Aligning Illumina-sequenced reads to the *P. grisea* genome allowed screening for single nucleotide variants (SNVs) that were homozygous in the *hu* pool but not in the WT sibling pool. We scored these SNVs for predicted functional consequences on annotated gene transcripts using SnpEff (Cingolani et al., 2012). Out of eight such SNVs, one was a G-to-A mutation in a 3' splice site of Phytri09g010120, which encodes an APETALA2 (*AP2*)-like transcription factor (**Figure 5E; Supplemental Table S6**). Co-segregation analysis in M3 families confirmed association of this mutation with the *hu* phenotype (**Supplemental Table S7**), and sequencing RT-PCR products of Phytri09g010120 from *hu* floral tissue showed mis-splicing in the 4th intron, resulting in partial skipping of exon 5 (**Figure 5E**). Importantly, independent CRISPR generated mutations of this *AP2-like* gene in *P. grisea* resulted in independent mutations that caused the same phenotype as *hu* (**Figure 5F**).

HU is the homolog of *Petunia hybrida* *AP2B/BLIND ENHANCER* (*BEN*) (**Figure 5G**), which specifies 2nd and 3rd floral whorl identity (Morel et al., 2017) with its redundant paralog *BROTHER OF BEN* (*BOB*). Petal development is strongly inhibited in *ben bob* double mutants, resulting in severely reduced or absent petals, and partial conversion of sepals into petals, resembling *hu* (Morel et al., 2017). Because the *Petunia hybrida* genome is highly fragmented (Bombarely et al., 2016), we performed a synteny analysis of the chromosomal segments containing *BOB* in *P. grisea*, *P. pruinosa*, and *S. lycopersicum* and found that this paralog of *HU* (*BEN*) is present in tomato but not in groundcherry (**Figure 5H**). Thus, *hu* emerged in our forward genetics mutagenesis screen, because the *BOB* ortholog and therefore redundancy is absent in *P. grisea*.

The first floral whorl of *hu* displays characteristics of both sepals and petals (**Figure 5I, J**). The whorl begins developing with green as the dominant color, like sepals, but gradually turns yellow as the flower matures, maintaining green color at organ tips. Nectar guides are also visible throughout development of the first whorl, indicative of early petal identity. After fertilization, the first whorl mildly increases in size but fails to fully inflate before gradually senescing as *hu* fruits develop into the size of WT fruits.

To characterize the role of *HU* in whorl identity and ICS, we profiled transcriptomes by RNA-seq from WT sepals and petals at two stages of organ maturation and compared them with corresponding stages of *hu* first whorls (**Figure 5K, and Methods**). Principal component analysis (PCA) revealed *hu* expression profiles (denoted as *hu*-PeSe) were positioned between the profiles of WT sepals and petals at both stages, supporting the mixed-organ identity observed phenotypically. Thus, the loss of the inflated calyx in *hu* mutants is from a failure to properly specify sepal and petal identity as opposed to directly disrupting a mechanistic origin of ICS. Our identification of *hu* through forward genetics exemplifies how presence-absence variation of paralogs can shape genetic redundancies and genotype-to-phenotype relationships in related lineages, and further illustrates the value of multiple related model systems.

DISCUSSION

Discoveries in plant development, cell biology, and genetics continue to depend on a limited number of model systems, often centered around *Arabidopsis thaliana* and its relatives in the Brassicaceae family (Chang et al., 2016). New models are essential to advance fundamental and

applied research beyond the small amount of biological diversity captured by current models. While additional model species have been proposed or are under development (Chang et al., 2016), most lack the powerful combination of efficient genomics and genetics. Moreover, emphasis is largely on neglected lineages and single representative species within them. An approach with complementary benefits relies on multiple models within a lineage to address often overlooked questions of species-specific and comparative evolutionary history over short time frames. The *Solanaceae* family is ideal in this regard, including: i) rich diversity throughout ~100 genera and more than 3000 species spanning ~30 million years of evolution; ii) broad agricultural importance from more than two dozen major and minor fruit and vegetable crops; and iii) feasibility of rapidly developing and integrating genome editing with reference and pangenome resources.

By establishing high-quality chromosome-scale assemblies for *P. grisea* and *P. pruinosa*, we developed these *Physalis* species as new models to advance *Solanaceae* systems with genomics and genetics. Most significantly, our integration of these resources revealed that the mechanisms underlying ICS remain elusive. Indeed, despite previous evidence suggesting otherwise, we conclude that none of the 11 candidate MADS-box genes we functionally characterized using genome editing, nor fertility alone, are core regulators of ICS. Our findings therefore force a reset in the search for the physiological, genetic, and molecular mechanistic origins of this evolutionary novelty. Though a logical starting point, the candidate gene approach based on MADS-box overexpression phenotypes in other species was prone to misleading hypotheses and false positives, likely due to the complex evolutionary history of the MADS-box family members and their even more complex genetic and physical interactions. Indeed, multiple MADS-box genes appear to be capable of mimicking ICS through overexpression, possibly due to coordinated activation of closely related paralogs and subsequent complex feedback regulation and interactions among other family members. This might suggest double and higher order mutants of these or other MADS-box genes not investigated here would ultimately perturb ICS, possibly reflecting a collective role of multiple family members acting redundantly or in a network. However, such a result would not necessarily indicate direct roles for these genes in the evolutionary steps leading to ICS.

Based on our genetics, we expect additional or other genes and molecular programs are central, and the tools established here provide the foundation to revisit ICS in an unbiased way.

ICS is a rapid and dynamic process, where extraordinary morphological changes in sepal growth and inflation occur within a few days. This suggests that the molecular events driving and responding to the inception of the transition from a non-inflated sepal whorl to active inflation may be short-lived, happening in the order of hours. We propose that the future dissection of ICS should be based on detailed and integrated temporal, morphological and molecular analyses to capture these transient events. A recent study in tomato took advantage of transcriptome profiling and computational ordering of hundreds of single shoot apical meristems to capture and reconstruct a highly detailed temporal gene expression map of the floral transition. These data revealed previously hidden gene, short-lived expression programs and several genes that function in parallel transient pathways critical to the floral transition process (Meir et al., 2021). With the new reference genomes and annotations of *P. grisea* and *P. pruinosa*, a similar approach can be applied to ICS, where large numbers of individual sepals can readily and reliably be harvested and profiled throughout calyx development. As opposed to focusing on entire floral buds (H. Gao et al., 2020), such high-resolution temporal transcriptome profiling of sepals alone would provide comprehensive and unbiased information regarding global and possibly gene-specific molecular signatures in the initiation and maintenance of inflation, and expose new candidates that can be studied using the integrated genomics and genome editing strategies demonstrated here.

Beyond floral development and ICS in *Physalis*, our work sets a high-quality anchor to broaden biological questions and discoveries in the *Solanaceae*, and further illustrates fast and efficient approaches to building new model systems. Establishing new pangenome and genome editing tools in many additional genera of *Solanaceae* and of other plant families will enable comparative genomic and genetic studies over both short and long evolutionary timescales.

MATERIALS AND METHODS

Plant material, growth conditions and phenotyping

Seeds of *Physalis grisea* and *Physalis pruinosa* were obtained from the Solanaceae Germplasm Bank at the Botanical Garden of Nijmegen and from commercial seed sources. Seeds were directly sown into soil (PRO-MIX BX Mycorrhizae Growing Mix) in 96-well plastic flats and grown in the greenhouse under long-day conditions (16-hr light/8-hr dark) supplemented with artificial light from high-pressure sodium bulbs ($\sim 250 \mu\text{mol m}^{-2} \text{s}^{-1}$). The temperature ranged

from 26-28°C during the day to 18-20°C during the night, with a relative humidity of 40%–60%. 4-week old seedlings were transplanted to 4 L pots filled with soil (PRO-MIX HP Mycorrhizae Growing Mix) in the same greenhouse, or into the fields at Cold Spring Harbor Laboratory (CSHL) unless otherwise noted. The tomato mutant displaying enlarged fleshy sepals from **Figure 4** was a gift from Dr. Dani Zamir, which arose from the whole genome backcross lines constructed from a cross between *Solanum pimpinellifolium* (LA1589) and *Solanum lycopersicum* inbred variety cv. E6203 (TA209) (Grandillo & Tanksley, 1996). Branching and internode length phenotypes were assayed in greenhouse-grown plants 2 months after sowing.

Extraction of high-molecular weight DNA and long-read sequencing

For long-read sequencing, shoot apices of 3-week old seedlings were harvested after a 48-h dark treatment. Extraction of high-molecular weight genomic DNA, construction of Oxford Nanopore Technology (ONT) libraries and PacBio HiFi libraries, and sequencing were described previously (Alonge et al., 2020, 2021). Hi-C experiments were conducted at Arima Genomics (San Diego, CA) from 2 g of flash-frozen leaf tissue.

***P. grisea* chloroplast and mitochondria genome assembly**

To assemble the *P. grisea* chloroplast genome, all HiFi reads were aligned to the previously published *Physalis* chloroplast reference genome (GenBank ID MH019243.1) with Minimap2 (v2.17-r974-dirty, -k19 -w19) (H. Li, 2018). All reads with at least one primary alignment spanning at least 90% of the read were assembled with HiCanu (v2.0, genomeSize=155k) (Nurk et al., 2020). The three resulting HiCanu unitigs were aligned to themselves with Nucmer (v3.1, -maxmatch) (Kurtz et al., 2004) and manually joined to produce a single trimmed and circularized contig. The contig was rotated to start at the same position as the reference. Liftoff was used to annotate the *P. grisea* chloroplast genome (Shumate & Salzberg, 2021).

P. grisea mitochondrial contigs were extracted from the polished ONT Flye assembly (see below). To identify mitochondrial contigs, tobacco (*Nicotiana tabacum*), pepper (*Capsicum annuum*), tomato (*Solanum lycopersicum*), and eggplant (*Solanum melongena*) mitochondrial transcript sequences (GenBank IDs NC_006581.1, NC_024624.1, NC_035963.1, and NC_050334.1, respectively) (Sugiyama et al., 2005) were extracted with gffread (G. Pertea & Pertea, 2020) and aligned to the ONT Flye assembly with Minimap2 (v2.17-r941, -x splice). For

each query transcriptome, any ONT contig shorter than 500 kbp with at least one alignment at least 100 bp long was considered, and any such contig identified by at least two query transcriptomes was labeled as mitochondrial. These contigs were aligned to the *P. grisea* chloroplast genome which indicated that they were all mitochondrial and not chloroplast sequences. These ONT mitochondrial sequences were aligned to the raw HiCanu contigs (see below) with Nucmer (v3.1, --maxmatch), and nine ONT contigs were manually replaced with two homologous HiCanu contigs. Liftoff was used to annotate the *P. grisea* mitochondrial genome using the *S. melongena* annotation as evidence.

***P. grisea* genome assembly**

P. grisea HiFi reads were assembled with HiCanu (v2.0, genomeSize=1500m). *P. grisea* ONT reads at least 38 kbp long and with an average quality score of at least Q12 were assembled with Flye (v2.8.1-b1676, --genome-size 1.5g) (Kolmogorov et al., 2019). The Flye contigs were iteratively polished for two rounds with Freebayes (Garrison & Marth, 2012). 200,000,000 Illumina short reads (SRA ID SRR7066586) were randomly sampled with seqtk (<https://github.com/lh3/seqtk>) and aligned to the Flye contigs with BWA-MEM (v0.7.17-r1198-dirty) (H. Li, 2013). Alignments were sorted and indexed with samtools [(Patro et al., 2017). Freebayes was used to call variants (v1.3.2-dirty, --skip-coverage 480) and polishing edits were incorporated with bcftools consensus (-i'QUAL>1 && (GT="AA" || GT="Aa")' -Hla) (Danecek et al., 2021).

The HiCanu contigs were aligned to the *P. grisea* chloroplast and mitochondria genomes with minimap2 (v2.17-r941, -x asm5), and any contigs covered more than 50% by alignments were removed. Potential bacterial contaminant sequences were screened out using a process similar to that used by the Vertebrate Genomes Project (Rhie et al., 2021). The HiCanu contigs were first masked with windowmasker (v1.0.0, -mk_counts -sformat obinary -genome_size 1448242897) (Morgulis et al., 2006). Then, the HiCanu contigs were aligned to all RefSeq bacterial genomes (downloaded on May 21, 2020) with BLAST (v2.5.0, -task megablast -outfmt "6 std score" -window_masker_db) (Altschul et al., 1990). Any contigs with at least one alignment with an E-value less than 0.0001, a score of at least 100, and a percent-identity of at least 98% were manually inspected, and one contig was removed. To remove potential false haplotypic duplication, HiFi reads were aligned to the screened contigs with Minimap2 (v2.17-

r941, -x asm5), and any contigs with at least 50% of the contig with less than 5X coverage were purged (Guan et al., 2020)

The screened and purged contigs were patched with Grafter (<https://github.com/mkirsche/Grafter>), a beta version of RagTag “patch” (Alonge et al., 2021). Polished ONT contigs were aligned to the HiCanu contigs with Nucmer (v3.1, -maxmatch -l 100 -c 500) and these alignments were used by Grafter to make patches (minq=0 min_weight_supp=10 min_weight=10). Patched contigs were then scaffolded with Bionano optical maps generated at the McDonnell Genome Institute at Washington University. Finally, chromosome-scale scaffolds were manually derived with Hi-C using Juicebox Assembly Tools (Dudchenko et al., 2018). To identify and correct potential misassemblies, HiFi and ONT reads were aligned to the scaffolds with Winnowmap (v1.11, -ax map-pb and -ax map-ont, respectively) and structural variants (SVs) were called with Sniffles (v1.0.12, -d 50 -n -l -s 3) (Jain, Rhie, Zhang, et al., 2020). We removed any SVs with less than 30% of reads supporting the alternative (ALT) allele and we merged the filtered SV calls with Jasmine (v1.0.10, max_dist=500 spec_reads=3 --output_genotypes) (Kirsche et al., 2021). After merging and manually inspecting the SV calls, a total of four misassemblies were manually corrected. VecScreen did not identify any “strong” or “moderate” hits to the adaptor contamination database (ftp://ftp.ncbi.nlm.nih.gov/pub/kitts/adaptors_for_screening_euks.fa) (<https://www.ncbi.nlm.nih.gov/tools/vecsreen/>). Finally, we removed any unplaced contigs shorter than 1 kbp. Mercury was used to compute QV and completeness metrics (k=21) (Rhie et al., 2020).

***P. pruinosa* genome assembly**

The *P. pruinosa* genome was assembled just as the *P. grisea* genome, with the following distinctions. HiFi reads were assembled with Hifiasm instead of HiCanu (v0.13-r308, -l0) (Cheng et al., 2021). Also, neither a chloroplast nor a mitochondria genome was assembled for *P. pruinosa*. To screen organellar contigs, raw Hifiasm primary contigs were aligned to the *P. pruinosa* reference chloroplast genome (GenBank ID MH019243.1) and the *P. grisea* mitochondria genome. As with *P. grisea*, SVs were called to identify potential misassemblies, and no misassemblies were found in the *P. pruinosa* scaffolds.

Gene and repeat annotation

Raw RNASeq reads from *P. grisea* were assessed for quality using FastQC v0.11.9 (FastQC, 2015), and were then aligned to the *P. grisea* assembly using STAR aligner (Dobin et al., 2013). Finally, reference-based transcripts were assembled using StringTie v2.1.2 (M. Pertea et al., 2015). We used the portcullis v1.2.0 (Mapleson et al., 2018) method to filter out the invalid splice junctions from the bam alignments. Additionally, we lifted orthologs from the Heinz ITAG4.0 annotation (Hosmani et al., 2019) and the pang genome annotation (L. Gao et al., 2019) using the Liftoff v1.6.1 (-exclude_partial -copies) (Shumate & Salzberg, 2021) pipeline. Structural gene annotations were then generated using the Mikado v2.0rc2 (Venturini et al., 2018) framework using the evidence set mentioned above following the Snakemake-based pipeline, [Daijin]. Functional annotation of the Mikado gene models was identified using the blastp alignments to uniprot/swissprot (Bairoch & Apweiler, 2000), TREMBL, Heinz ITAG4.0, and pan genome proteins database (L. Gao et al., 2019; Hosmani et al., 2019) and transferred using the AHRD pipeline (<https://github.com/asishallab/AHRD>). The *P. pruinosa* assembly was gene-annotated with Liftoff, using the *P. grisea* gene annotation as evidence (-copies). Transposable elements were annotated with EDTA (v1.9.6, --sensitive 1 --anno 1 --evaluate 1 --cds) (Ou et al., 2019). BUSCO was run on each genome assembly using the “embryophyta_odb10” lineage database (v5.0.0, -e 1e-05 --augustus --long) (Simão et al., 2015).

Structural variant detection

Structural variation between *P. grisea* and *P. pruinosa* was identified using the same pipeline used to identify structural variant-like misassemblies described above. However, instead of aligning *P. grisea* reads to the *P. grisea* assembly and *P. pruinosa* reads to the *P. pruinosa* assembly, *P. grisea* reads were aligned to the *P. pruinosa* assembly and *P. pruinosa* reads were aligned to the *P. grisea* assembly. Also, Winnowmap2 (v2.0) was used instead of Winnowmap for alignments (Jain, Rhie, Hansen, et al., 2020). SVs intersecting genomic features in **Figure 1G** were counted as previously described (Alonge et al., 2020) based on *P. grisea* annotation v1.3.0

CRISPR-Cas9 mutagenesis, plant transformation, and selection of mutant alleles

CRISPR-Cas9 mutagenesis was performed following our protocol as previously described (Lemmon et al., 2018; Swartwood & Van Eck, 2019). Gene IDs related to this study are listed in

Supplemental Table S8. Briefly, guide RNAs (gRNAs) were designed to be used in the Golden Gate cloning system (all gRNAs used in this study are listed in **Supplemental Table S9** and were assembled into Level 1 (L1) constructs under the control of the U6 promoter. L1 guide constructs were then assembled with Level 1 constructs pICH47732-*NOS_{pro}:NPTII* and pICH47742-*35S_{pro}:Cas9* into the binary Level 2 vector pAGM4723. The final binary vectors were then transformed into groundcherry by *Agrobacterium tumefaciens*-mediated transformation through tissue culture (Swartwood & Van Eck, 2019). Multiple independent first-generation transgenic plants (T₀) were genotyped with specific primers surrounding the target sites. T₀ plants were self-pollinated and the T₁ generation was genotyped for the target genes and the presence or absence of the CRISPR-Cas9 transgene. We noticed that tissue culture and transformation resulted in a variable frequency of tetraploidy. All mutants were verified as homozygous or biallelic and having only mutant alleles.

Tissue collection, RNA extraction, RT-PCR and RT-qPCR

All tissues used were immediately frozen in liquid nitrogen before RNA extraction. For the analysis of *ANI* transcripts in *P. grisea* and *P. pruinosa*, young flower buds were harvested. For *TAGL1* gene expression analysis in the tomato calyx mutant, developing sepals at the open flower stage were harvested. Sepal tissue from three different WT plants, and from four different mutant plants were assayed as three biological replicates and four biological replicates respectively. For the analysis of *huskless* (*hu*) and WT sepal gene expression profiles, the first whorl of *hu*, and WT sepals and petals at the stages shown in **Figure 5K** were harvested. Total RNA was extracted with the Zymo Research Quick-RNA Microprep kit following the manufacturer's protocol. cDNA synthesis was performed using SuperScript IV VILO Master Mix (Thermal Fisher) with 500 ng to 1,500 ng total RNA input. RT-PCR was performed with KOD OneTM PCR Master Mix and primers listed in **Supplemental Table S10**. RT-qPCR was performed using Fast SYBRTM Green Master Mix with primers listed in **Supplemental Table S10** on the Applied BiosystemsTM QuantStudio 6 system.

Transcriptome analysis of *huskless* and WT

RNA-seq and differentially expressed genes (DEGs) analyses were performed as previously described with slight modification (Kwon et al., 2022). Briefly, the libraries for RNA-seq were

prepared by the KAPA mRNA HyperPrep Kit (Roche). Paired-end 150-base sequencing was conducted on the Illumina sequencing platform (NextSeq, High-Output). Reads for WT and *hu* were trimmed by quality using Trimmomatic (Bolger et al., 2014) (v.0.39, parameters: ILLUMINACLIP:TruSeq3-PE-2.fa:2:40:15:1:FALSE LEADING:30 TRAILING:30 MINLEN:50) and quantified to the reference transcriptome assembly of *P. grisea* v1.3.2 using Salmon v1.4.0 (Patro et al., 2017). Quantification results from Salmon were imported into R using tximport v1.24.0 (Soneson et al., 2016). PCA analysis of samples were performed and plotted using DEseq2 v1.36.0 (Love et al., 2014) and pcaExplorer v2.22.0 (Marini & Binder, 2019) with counts of the top 3000 variable genes.

Mapping of the yellow nectar guide variant

The yellow-guide trait displayed classical patterns of Mendelian inheritance of a single recessive gene in the F1 and F2 populations from the cross between *P. grisea* and *P. pruinosa*. A bulk segregant analysis (BSA) was performed using 20 plants from each of the yellow-guide pool and purple-guide pool in the F2 segregating population. All reads were assessed for overall quality by FastQC v0.11.9 (FastQC, 2015). Read mapping, variant calling, and SNP-index calculation of the Illumina reads from each pool was done by QTL-seq v2.2.2 (Takagi et al., 2013). Parameters used for the sliding window SNP-index calculation by the qtlplot command were -n1 20 -n2 20 -F 2 -D 250 -d 5 -w 1000 -s 50. The calculated SNP-index in each sliding window was imported into R (R Core Team, 2020) for the final plot.

EMS mutagenesis and mutant screening in *P. grisea*

A small-scale EMS mutagenesis was performed using approximately 1500 *P. grisea* seeds (measured by weight). Seeds were soaked in distilled water overnight and then treated with 0.2% EMS (ethyl methanesulfonate, Sigma Aldrich) for 6 h. After treatment, seeds were washed with distilled water thoroughly and sowed into 96-well flats. 4-week-old seedlings were then transplanted into the field. When harvesting, fruits from every four M₁ plants were bulk harvested into one group. For mutant screening, 80 groups of M₂s were sowed, transplanted, and screened for sepal related phenotypes.

Mapping of *huskless*

Three *huskless* phenotype plants were identified from the same group. The pooled DNA from the three mutants, and the pooled DNA from 30 WT-looking siblings from the same group, were obtained by CTAB extraction methods. Libraries were prepared for sequencing using the Kapa Hyper PCR-free Kit and sequenced on Illumina Nextseq (PE150, high output). All reads were assessed for overall quality by FastQC v0.11.9 (FastQC, 2015), and trimmed with Trimmomatic v0.39 (Bolger et al., 2014) with parameters ILLUMINACLIP:TruSeq3-PE.fa:2:40:15:1:FALSE LEADING:30 TRAILING:30 MINLEN:75 TOPHRED33. Trimmed paired reads were mapped to the reference *P. grisea* genome using BWA-MEM (H. Li, 2013). Alignments were then sorted with samtools (H. Li et al., 2009). and duplicates marked with PicardTools (Picard Toolkit, 2019). Variants were called with freebayes (Garrison & Marth, 2012) and filtered with VCFtools (Danecek et al., 2011) for SNPs with minimum read depth of 3 and minimum quality value of 20. SNPs that are homozygous in the mutant pool but not homozygous in the WT sibling pool were analyzed for effects on transcripts with snpEff (Cingolani et al., 2012) with *P. grisea* annotation v1.3.0.

Molecular phylogenetic analyses

In order to determine the phylogenetic relationship between the eleven selected *Solanaceae* species, eighteen genomes were used to define orthogroups by Conservatory (Hendelman et al., 2021). Protein sequences of the twenty most conserved orthogroups genes were aligned with MAFFT (v7.487) FFT-NS-2 (Kato & Standley, 2013) (see **Supplemental Data Set S6**), before constructing the tree by IQ-tree with the following parameters -st AA -b 100 -pers 0.5 -wbtl (Minh et al., 2020). For the phylogenetic analysis of AP2-like proteins, protein sequences of the orthologs were retrieved from *P. grisea*, *S. lycopersicum* and *P. axillaris* by BLAST (Altschul et al., 1990). Protein sequences (see **Supplemental Data Set S7**) were imported in MEGA 11 (Tamura et al., 2021) and aligned with MUSCLE (default parameters). The tree was constructed using the maximum likelihood method and JTT matrix-based model. Bootstrap values (%) based on 500 replicates are indicated near the branching points; branches below 50% have been collapsed. Alignment and tree files are provided as **Supplemental Files S1 and S2**.

Synteny analysis at the *SIBOB* locus

Because the scaffold quality of the *P. axillaris* genome in the vicinity of *BOB* was suboptimal, we used SL4.0 with the *P. grisea* genome for the analysis. A BLAST search using *Petunia BOB* and *SlBOB* cDNA query sequences against the *P. grisea* genome failed to retrieve a high-confidence hit other than Phygr10g010120, which is the *BEN* ortholog. BLAST search of genes upstream and downstream of *SlBOB* located their syntenic regions in the *P. grisea* genome. Genomic sequences with annotations from Solyc10g084240 ~ Solyc10g084420, and from Phygr10g011780 ~ Phygr10g011960 were used in clinker v0.0.23 (Gilchrist & Chooi, 2021) to generate gene translation alignments and visualizations.

Accession numbers

Genome assemblies and annotations are available at <https://github.com/pan-sol/pan-sol-data/tree/main/Physalis>. Raw sequence data from this article can be found in Sequence Read Archive (SRA) under the BioProject PRJNA862958.

Supplemental data

Supplemental Figure S1. Hi-C heatmaps confirm reference assembly structural accuracy.

Supplemental Figure S2. Illustrations of CRISPR-engineered mutations in this study.

Supplemental Figure S3. Maximum likelihood consensus tree of the euAP2 proteins from *A. thaliana*, *P. axillaris*, *S. lycopersicum*, and *P. grisea*.

Supplemental Table S1. Genome assembly statistics.

Supplemental Table S2. Annotation stats of *P. grisea* and *P. pruinosa* genomes.

Supplemental Table S3. Result summary of SNP calls of *P. pruinosa* Illumina reads against *P. grisea* as reference.

Supplemental Table S4. High impact SNP calls of *P. pruinosa* Illumina reads against *P. grisea* as reference.

Supplemental Table S5. SVs intersecting CDS.

Supplemental Table S5. SVs intersecting genes.

Supplemental Table S6. SNPs with predicted high impact on transcripts of *huskless*.

Supplemental Table S7. Co-segregation test of the G/A SNP in Phygri09g010120 and the huskless phenotype.

Supplemental Table S8. Genes related to work in this study.

Supplemental Table S9. CRISPR guides used in this study.

Supplemental Table S10. Primers used in this study.

Supplemental Data Set S1. Internode length measurement of *P. grisea* and *P. pruinosa* related to **Figure 1B, C**.

Supplemental Data Set S2. SVs intersecting genes.

Supplemental Data Set S3. CRISPR-generated mutations in this study.

Supplemental Data Set S4. Branching phenotype counts for WT, *Pgmpf2* and *Pgmpf3* related to **Figure 3F**.

Supplemental Data Set S5. Calyx length and width measurement of WT, *Pgmpf2* and *Pgmpf3* related to **Figure 3G**.

Supplemental Data Set S6. Protein sequences used for the phylogenic analysis of Solanaceae species in **Figure 1A**.

Supplemental Data Set S7. Protein sequences used for the phylogenetic analysis of AP2-like proteins in **Figure 5G**.

Supplemental Data Set S8. Statistical analysis tables.

Supplemental File S1. Tree file for the phylogenetic analysis in **Figure 1A**.

Supplemental File S2. Tree file for the phylogenetic analyses in **Figure 5G** and **Supplemental Figure S3**

Acknowledgements

We thank Yuval Eshed and members of the Van Eck, Schatz, and Lippman labs for helpful discussions. We thank R. Santos, B. Semen, and G. Robitaille from the Lippman lab for technical support. We thank A. Horowitz Doyle, K. Swartwood, M. Tjahjadi, L. Randall and P. Keen from the Van Eck laboratory for transformations. We thank T. Mulligan, K. Schlecht, A. Krainer, S. Qiao, and B. Fitzgerald for assistance with plant care. We thank D. Zamir for providing the tomato ICS mimic mutant. We also thank Yueqin Yang for assistance with the EMS mutagenesis screen, Adina Lippman for suggestions on writing, and Katie Jenike from the

Schatz laboratory for assistance with bioinformatics. This work was funded by the Howard Hughes Medical Institute to Z.B.L., and the National Science Foundation Plant Genome Research Program (IOS-1732253) to J.V.E., M.C.S., and Z.B.L. Conflict of interest statement: None declared.

Author contributions

M.C.S., and Z.B.L. conceived, designed, and led the study, and analyzed the data. J.H. led and coordinated the experiments and analyses. M.C.S. and Z.B.L. performed the genome sequencing, M.A. and M.C.S. generated the genome assemblies. S.R. annotated the genomes. M.B. and S.S. prepared DNA for long-read sequencing. S.S. performed the genome sequencing and analysis to identify the tomato ICS mimic mutation. N.T.R. contributed the CRISPR construct targeting *PgMPF3*. J.V.E. led the CRISPR transformations and generated all the CRISPR T₀ lines. A.H. contributed to the phylogenetic analyses. J.H., M.A. and Z.B.L. prepared the figures and wrote the manuscript. All authors read, edited and approved the manuscript.

FIGURE LEGENDS

Figure 1. Reference-quality genome assemblies of *P. grisea* and *P. pruinosa*.

A. Phylogeny of selected *Solanaceae* species based on the 20 most conserved protein sequences (see **Methods**). **B.** Whole plant images of *P. grisea* and *P. pruinosa* 40 d after sowing (DAS) in greenhouse conditions. Bar = 10 cm. **C.** Sympodial shoot architectures of *P. grisea* and *P. pruinosa*. Quantification of internode lengths is in **Supplemental Data Set S1**. Bar = 5 cm. **D.** Images of *P. grisea* and *P. pruinosa* calyces and fruits at different stages of development. Husks were manually opened to show fruits. Bar = 2 cm. **E.** Circos plots comparing *P. grisea* and *P. pruinosa* genomes. Circos quantitative tracks are summed in 100-kbp windows and show the number of genes (lower tick = 0, middle tick = 25, higher tick = 49), LTR retrotransposons (lower tick = 0, middle tick = 102, higher tick = 204) and SVs (lower tick = 0, middle tick = 4, higher tick = 9). The inner ribbon track shows whole genome alignments, with blue indicating forward-strand alignments and red indicating reverse-strand alignments (inversions). Darker colors indicate alignment boundaries. **F.** Distribution of deletion and insertion SVs between 30 bp and 10 kbp from *P. pruinosa* compared to *P. grisea*, summed in 200-bp windows. **G.** Counts of SVs intersecting genomic features, comparing *P. pruinosa* to *P. grisea*.

Figure 2. Loss of purple pigmentation in *P. pruinosa* is due to an intronic SV in the bHLH transcription factor gene *ANTHOCYANIN1*.

A. Images showing the difference in pigmentation between *P. grisea* and *P. pruinosa*. Arrows point to purple (*P. grisea*) compared to yellow (*P. pruinosa*) pigmentation on stems and flowers. Top bars = 1 cm; bottom bars = 2 mm. **B.** Mapping by sequencing showing the Δ SNP-index across all twelve chromosomes using *P. grisea* as the reference, with SNP ratios between yellow-guide and the purple-guide pools from an interspecific F2 population. Yellow line: 95% confidence interval cut-offs of Δ SNP-index. **C.** Simplified pathway of anthocyanin biosynthesis based on data from petunia. Major transcriptional and enzymatic regulators are shown as abbreviations. PAL: Phenylalanine Ammonialyase; C4H: Cinnamate 4-Hydroxylase; 4CL: 4-Coumaroyl-CoA ligase; CHS: Chalcone Synthase; CHI: Chalcone Isomerase; F3H: Flavanone 3-hydroxylase; F3'H: Flavonoid 3'-hydroxylase; AN1: ANTHOCYANIN 1; AN2: ANTHOCYANIN 2; AN11: ANTHOCYANIN 11; DFR: Dihydroflavonol Reductase; ANS: Anthocyanin Synthase. Dashed lines indicate multiple steps condensed. Bold red font indicates components of the MYB-bHLH-WD40 (MBW) complex that transcriptionally activates late biosynthetic genes. **D.** Top: The Δ SNP-index plot for chromosome 4. The black arrow points to the genomic location of the *ANI* candidate gene. Bottom: a composite of Illumina mapped-reads from *P. pruinosa* at the 2nd intron of *ANI* showing a 43-bp deletion in all *PpANI* (*Phypru04g010390*) sequences. In all gene models (including later figures), deep blue boxes, black lines, and light blue boxes represent exonic, intronic, and untranslated regions, respectively. **E.** Molecular consequences of the 43-bp intronic deletion in *PpANI* revealed by RT-PCR and sequencing. Red arrows indicate the forward and reverse RT-PCR primers. Longer amplicons and thus *ANI* transcripts from both the yellow-guide F2 bulk pool and *P. pruinosa* were identified by agarose gel electrophoresis. Sanger sequencing revealed the inclusion of a 179-bp fragment of intron 2 in the *PpANI* amplicon, resulting in a premature stop codon. Red box reflects intronic sequence retained in the transcript. Black asterisk, premature stop. **F.** Loss of purple pigmentation in CRISPR edited *PgANI* T₀ plants. Left bar = 2 cm; right bar = 5 mm. **G.** CRISPR-Cas9 generated mutant alleles from the yellow T₀ chimeric plants are shown. Red dashed lines represent deletions. The red bold letter indicates a single nucleotide insertion.

Figure 3. CRISPR-Cas9 generated mutants of the MADS-box genes *PgMPF2* and *PgMPF3* do not prevent ICS.

A. Images showing sequential stages of ICS in *P. grisea* from early flower formation to calyx inflation over 3 d. Bar = 10 mm. **B.** Multiple, independently derived null alleles in *PgMPF2* and *PgMPF3*. Red boxes and lines, deletions; black asterisks, stop codons. Three alleles of *PgMPF2* (*Pgmpf2*^{CR-1}, *Pgmpf2*^{CR-2}, *Pgmpf2*^{CR-3}) with different mutations in exon 3 result in the same premature stop codon. Specific mutations for all alleles are shown in **Supplemental Figure S2** and in **Supplemental Data Set S3**. **C-G.** Phenotypes of *Pgmpf2* and *Pgmpf3* null mutants. All homozygous mutants independently derived alleles showed the same phenotypes, and *Pgmpf2*^{CR-5} and *Pgmpf3*^{CR-1} were used as references for phenotypic analyses. **C.** Calyx inflation is not disrupted in *Pgmpf2* and *Pgmpf3* mutants. Representative images from *Pgmpf2*^{CR-5} and *Pgmpf3*^{CR-1} are shown. The leaf-like sepal tip of *Pgmpf3*^{CR-1} is indicated by the red arrow. Bar = 10 mm. **D** and **E.** Shoot branching phenotype of *Pgmpf3*^{CR-1} compared to WT. A typical sympodial unit of WT *Physalis* consists of one leaf, one flower and two side shoots. *Pgmpf3* mutants develop mostly three side shoots. Bar = 10 mm. **(E).** Branches are indicated by red arrows in representative images. **F.** Quantification of branching in WT, *Pgmpf2* and *Pgmpf3* shown as stacked bar charts. Branching counts are shown in **Supplemental Data Set S4**. **G.** Quantification of calyx height/width ratio in WT, *Pgmpf2* and *Pgmpf3*. Raw measurements are shown in **Supplemental Data Set S5**. Statistical significance determined by two-tailed, two-sample *t*-tests, and *p* values are shown. **H.** Calyx inflation is not disrupted in *Pgmpf2* *Pgmpf3* double mutants. Two allelic combinations in double mutants of *Pgmpf2* *Pgmpf3* (*a1* and *a2*) displayed the same phenotype, and allele *a2* was used as reference in the image shown. Bar = 10 mm.

Figure 4. CRISPR-Cas9 generated mutations in eight additional candidate MADS-box genes do not disrupt ICS.

A. Overexpression of *SITAGLI* caused by a transposable element insertion (see **Methods**) results in an enlarged calyx in tomato, mimicking ICS and presenting another candidate MADS-box gene. Left: image of calyx phenotype from the *SITAGLI* mutant. Bar = 10 mm. Right, top: gene model of *SITAGLI* with the transposon insertion (black triangle) identified by genome sequencing. Right, bottom: RT-qPCR on cDNA derived from young sepals showing

overexpression of *SITAGLI* in the mutant. Sepal tissue from three WT plants, and from four mutant plants were assayed (see **methods**); each data point represents one technical replicate. **B.** Mutations in *PgTAGLI* and *PgTAGI* cause homeotic transformations of stamens to petal-like organs but do not disrupt ICS. Middle image: representative calyx phenotypes at different developmental stages. Bar = 10 mm. Right image: single organs from the 3rd floral whorl. Bar = 2 mm. **C.** Mutations in three *SEP4* homologs do not disrupt ICS. Bar = 10 mm. **D.** Mutations in multiple B-function MADS-box genes do not disrupt ICS. Bar = 10 mm. **E.** ICS still occurs in mutants with fertilization defects or those that fail to produce fruits. Mutations in *PgTAGI*, *PgTAGLI*, *PgDEF*, and *PgGlo1* cause homeotic transformations of floral organs that abolish self-fertilization, but ICS is preserved. Bar = 5 mm.

Figure 5. The *huskless* mutant lacks an inflated calyx due to mutation of an *AP2*-like transcription factor. A-D. Phenotypes of the EMS-derived *huskless* (*hu*) mutant. **A** and **B.** Images of WT and the *hu* mutant displaying the loss of calyx phenotype at the mature green fruit stage. Bar = 1 cm. **C** and **D.** Longitudinal SEM images of developing flowers of WT and *hu* showing *hu* mutants develop only three floral whorls compared to four in WT. The first whorl of *hu* flowers shows hallmarks of sepal and petal identity. Se: sepal; Pe: petal; St: stamen; Ca: Carpel. Bar = 0.5 mm. **E.** Gene model showing the G-to-A point mutation causing partial skipping of exon 5 in the *AP2*-like transcription factor gene *Phygri09g010120*. Blue-colored nucleotides represent exonic sequences; red boxes indicate 3' splice sites in WT and *hu*. **F.** CRISPR-Cas9 generated mutations in *Phygri09g010120*. Top: gene models showing three independent CRISPR null alleles of *hu*. Sequences 3' of the 3rd intron are omitted. *hu*^{CR-1} is homozygous for allele 1 (*a1*). Bottom: images of *hu*^{CR-1} flower phenotype. Bar = 2 mm. **G.** Maximum likelihood consensus tree of the TOE-type euAP2 proteins from *A. thaliana* (gene names in green), *P. axillaris* (Peaxi IDs in purple), *S. lycopersicum* (Solyc IDs in red), and *P. grisea* (Phygri IDs in black). Bootstrap values (%) based on 500 replicates are indicated near the branching points; branches below 50% have been collapsed. **H.** Local synteny analysis between *S. lycopersicum* and *P. grisea* showing the absence of the *Solyc10g084340* orthologue (petunia *BOB* orthologue) in *P. grisea*. Arrows indicate genes and orientations. Protein identity percentages between orthologues are indicated by ribbon shades in grayscale; only links above 80% identity are shown. **I** and **J.** Series of images of WT and *hu* developing flowers from before

anthesis through early fruit development. Bar = 5 mm. **K.** Principal component analysis (PCA) of WT and *hu* RNA-seq data. Right image: visual reference of the two stages used for expression profiling from WT and *hu* floral whorls. Numbers (-1 or -2) in the sample groups represent stage 1 or 2; petal or sepal whorls in WT are denoted as Pe, Se respectively; PeSe represents the merged outer whorl in *hu*. The top 3000 differentially expressed genes were used for PCA. Bar = 5 mm.

REFERENCES

- Alonge, M., Lebeigle, L., Kirsche, M., Aganezov, S., Wang, X., Lippman, Z. B., Schatz, M. C., & Soyk, S. (2021). Automated assembly scaffolding elevates a new tomato system for high-throughput genome editing. *BioRxiv*, 2021.11.18.469135.
<https://doi.org/10.1101/2021.11.18.469135>
- Alonge, M., Wang, X., Benoit, M., Soyk, S., Pereira, L., Zhang, L., Suresh, H., Ramakrishnan, S., Maumus, F., Ciren, D., Levy, Y., Harel, T. H., Shalev-Schlosser, G., Amsellem, Z., Razifard, H., Caicedo, A. L., Tieman, D. M., Klee, H., Kirsche, M., ... Lippman, Z. B. (2020). Major Impacts of Widespread Structural Variation on Gene Expression and Crop Improvement in Tomato. *Cell*, 182(1), 145-161.e23.
<https://doi.org/https://doi.org/10.1016/j.cell.2020.05.021>
- Altschul, S. F., Gish, W., Miller, W., Myers, E. W., & Lipman, D. J. (1990). Basic local alignment search tool. *Journal of Molecular Biology*, 215(3), 403–410.
[https://doi.org/https://doi.org/10.1016/S0022-2836\(05\)80360-2](https://doi.org/https://doi.org/10.1016/S0022-2836(05)80360-2)
- Añibarro-Ortega, M., Pinela, J., Alexopoulos, A., Petropoulos, S. A., Ferreira, I. C. F. R., & Barros, L. (2022). Chapter Four - The powerful Solanaceae: Food and nutraceutical applications in a sustainable world. In F. Toldrá (Ed.), *Advances in Food and Nutrition Research* (Vol. 100, pp. 131–172). Academic Press.
<https://doi.org/https://doi.org/10.1016/bs.afnr.2022.03.004>
- Bairoch, A., & Apweiler, R. (2000). The SWISS-PROT protein sequence database and its supplement TrEMBL in 2000. *Nucleic Acids Research*, 28(1), 45–48.
<https://doi.org/10.1093/nar/28.1.45>
- Baumann, T. W., & Meier, C. M. (1993). Chemical defence by withanolides during fruit development in *Physalis peruviana*. *Phytochemistry*, 33(2), 317–321.
[https://doi.org/https://doi.org/10.1016/0031-9422\(93\)85510-X](https://doi.org/https://doi.org/10.1016/0031-9422(93)85510-X)
- Bolger, A. M., Lohse, M., & Usadel, B. (2014). Trimmomatic: a flexible trimmer for Illumina sequence data. *Bioinformatics*, 30(15), 2114–2120.
<https://doi.org/10.1093/bioinformatics/btu170>

- Bombarely, A., Moser, M., Amrad, A., Bao, M., Bapaume, L., Barry, C. S., Bliet, M., Boersma, M. R., Borghi, L., Bruggmann, R., Bucher, M., D'Agostino, N., Davies, K., Druege, U., Dudareva, N., Egea-Cortines, M., Delledonne, M., Fernandez-Pozo, N., Franken, P., ... Kuhlemeier, C. (2016). Insight into the evolution of the Solanaceae from the parental genomes of *Petunia hybrida*. *Nature Plants*, 2(6), 16074. <https://doi.org/10.1038/nplants.2016.74>
- Chang, C., Bowman, J. L., & Meyerowitz, E. M. (2016). Field Guide to Plant Model Systems. *Cell*, 167(2), 325–339. <https://doi.org/10.1016/j.cell.2016.08.031>
- Cheng, H., Concepcion, G. T., Feng, X., Zhang, H., & Li, H. (2021). Haplotype-resolved de novo assembly using phased assembly graphs with hifiasm. *Nature Methods*, 18(2), 170–175. <https://doi.org/10.1038/s41592-020-01056-5>
- Cingolani, P., Platts, A., Wang, L. L., Coon, M., Nguyen, T., Wang, L., Land, S. J., Lu, X., & Ruden, D. M. (2012). A program for annotating and predicting the effects of single nucleotide polymorphisms, SnpEff. *Fly*, 6(2), 80–92. <https://doi.org/10.4161/fly.19695>
- Danecek, P., Auton, A., Abecasis, G., Albers, C. A., Banks, E., DePristo, M. A., Handsaker, R. E., Lunter, G., Marth, G. T., Sherry, S. T., McVean, G., Durbin, R., & Group, 1000 Genomes Project Analysis. (2011). The variant call format and VCFtools. *Bioinformatics*, 27(15), 2156–2158. <https://doi.org/10.1093/bioinformatics/btr330>
- Danecek, P., Bonfield, J. K., Liddle, J., Marshall, J., Ohan, V., Pollard, M. O., Whitwham, A., Keane, T., McCarthy, S. A., Davies, R. M., & Li, H. (2021). Twelve years of SAMtools and BCFtools. *GigaScience*, 10(2), giab008. <https://doi.org/10.1093/gigascience/giab008>
- Deanna, R., Larter, M. D., Barboza, G. E., & Smith, S. D. (2019). Repeated evolution of a morphological novelty: a phylogenetic analysis of the inflated fruiting calyx in the Physalideae tribe (Solanaceae). *American Journal of Botany*, 106(2), 270–279. <https://doi.org/10.1002/ajb2.1242>
- Deanna, R., Wilf, P., & Gandolfo, M. A. (2020). New physaloid fruit-fossil species from early Eocene South America. *American Journal of Botany*, 107(12), 1749–1762. <https://doi.org/10.1002/ajb2.1565>
- Dobin, A., Davis, C. A., Schlesinger, F., Drenkow, J., Zaleski, C., Jha, S., Batut, P., Chaisson, M., & Gingeras, T. R. (2013). STAR: ultrafast universal RNA-seq aligner. *Bioinformatics*, 29(1), 15–21. <https://doi.org/10.1093/bioinformatics/bts635>
- Dudchenko, O., Shamim, M. S., Batra, S. S., Durand, N. C., Musial, N. T., Mostofa, R., Pham, M., Glenn St Hilaire, B., Yao, W., Stamenova, E., Hoeger, M., Nyquist, S. K., Korchina, V., Pletch, K., Flanagan, J. P., Tomaszewicz, A., McAloose, D., Pérez Estrada, C., Novak, B. J., ... Aiden, E. L. (2018). The Juicebox Assembly Tools module facilitates de novo assembly of mammalian genomes with chromosome-length scaffolds for under \$1000. *BioRxiv*, 254797. <https://doi.org/10.1101/254797>
- FastQC*. (2015). <https://qubeshub.org/resources/fastqc>

916 Gao, H., Li, J., Wang, L., Zhang, J., & He, C. (2020). Transcriptomic variation of the flower–
 917 fruit transition in *Physalis* and *Solanum*. *Planta*, 252(2), 28.
 918 <https://doi.org/10.1007/s00425-020-03434-x>

919 Gao, L., Gonda, I., Sun, H., Ma, Q., Bao, K., Tieman, D. M., Burzynski-Chang, E. A., Fish, T.
 920 L., Stromberg, K. A., Sacks, G. L., Thannhauser, T. W., Foolad, M. R., Diez, M. J.,
 921 Blanca, J., Canizares, J., Xu, Y., van der Knaap, E., Huang, S., Klee, H. J., ... Fei, Z.
 922 (2019). The tomato pan-genome uncovers new genes and a rare allele regulating fruit
 923 flavor. *Nature Genetics*, 51(6), 1044–1051. <https://doi.org/10.1038/s41588-019-0410-2>

924 Garrison, E. P., & Marth, G. T. (2012). Haplotype-based variant detection from short-read
 925 sequencing. *ArXiv: Genomics*.

926 Gebhardt, C. (2016). The historical role of species from the Solanaceae plant family in genetic
 927 research. *Theoretical and Applied Genetics*, 129(12), 2281–2294.
 928 <https://doi.org/10.1007/s00122-016-2804-1>

929 Gilchrist, C. L. M., & Chooi, Y.-H. (2021). clinker & clustermap.js: automatic generation
 930 of gene cluster comparison figures. *Bioinformatics*, 37(16), 2473–2475.
 931 <https://doi.org/10.1093/bioinformatics/btab007>

932 Grandillo, S., & Tanksley, S. D. (1996). QTL analysis of horticultural traits differentiating the
 933 cultivated tomato from the closely related species *Lycopersicon pimpinellifolium*.
 934 *Theoretical and Applied Genetics*, 92(8), 935–951. <https://doi.org/10.1007/BF00224033>

935 Guan, D., McCarthy, S. A., Wood, J., Howe, K., Wang, Y., & Durbin, R. (2020). Identifying
 936 and removing haplotypic duplication in primary genome assemblies. *Bioinformatics*,
 937 36(9), 2896–2898. <https://doi.org/10.1093/bioinformatics/btaa025>

938 He, C., Münster, T., & Saedler, H. (2004). On the origin of floral morphological novelties.
 939 *FEBS Letters*, 567(1), 147–151.
 940 <https://doi.org/https://doi.org/10.1016/j.febslet.2004.02.090>

941 He, C., & Saedler, H. (2005). Heterotopic expression of MPF2 is the key to the evolution of
 942 the Chinese lantern of *Physalis*, a morphological novelty in Solanaceae. *Proceedings of*
 943 *the National Academy of Sciences of the United States of America*, 102(16), 5779–5784.
 944 <https://doi.org/10.1073/pnas.0501877102>

945 He, C., & Saedler, H. (2007). Hormonal control of the inflated calyx syndrome, a
 946 morphological novelty, in *Physalis*. *The Plant Journal*, 49(5), 935–946.
 947 <https://doi.org/https://doi.org/10.1111/j.1365-313X.2006.03008.x>

948 Hendelman, A., Zebell, S., Rodriguez-Leal, D., Dukler, N., Robitaille, G., Wu, X., Kostyun, J.,
 949 Tal, L., Wang, P., Bartlett, M. E., Eshed, Y., Efroni, I., & Lippman, Z. B. (2021).
 950 Conserved pleiotropy of an ancient plant homeobox gene uncovered by cis-regulatory
 951 dissection. *Cell*, 184(7), 1724–1739.e16.
 952 <https://doi.org/https://doi.org/10.1016/j.cell.2021.02.001>

- Hosmani, P. S., Flores-Gonzalez, M., van de Geest, H., Maumus, F., Bakker, L. v, Schijlen, E., van Haarst, J., Cordewener, J., Sanchez-Perez, G., Peters, S., Fei, Z., Giovannoni, J. J., Mueller, L. A., & Saha, S. (2019). An improved de novo assembly and annotation of the tomato reference genome using single-molecule sequencing, Hi-C proximity ligation and optical maps. *BioRxiv*, 767764. <https://doi.org/10.1101/767764>
- Hu, J.-Y., & Saedler, H. (2007). Evolution of the Inflated Calyx Syndrome in Solanaceae. *Molecular Biology and Evolution*, 24(11), 2443–2453. <https://doi.org/10.1093/molbev/msm177>
- Huang, M., He, J.-X., Hu, H.-X., Zhang, K., Wang, X.-N., Zhao, B.-B., Lou, H.-X., Ren, D.-M., & Shen, T. (2020). Withanolides from the genus *Physalis*: a review on their phytochemical and pharmacological aspects. *Journal of Pharmacy and Pharmacology*, 72(5), 649–669. <https://doi.org/10.1111/jphp.13209>
- Itkin, M., Seybold, H., Breitel, D., Rogachev, I., Meir, S., & Aharoni, A. (2009). TOMATO AGAMOUS-LIKE 1 is a component of the fruit ripening regulatory network. *The Plant Journal*, 60(6), 1081–1095. <https://doi.org/https://doi.org/10.1111/j.1365-313X.2009.04064.x>
- Jain, C., Rhie, A., Hansen, N., Koren, S., & Phillippy, A. M. (2020). A long read mapping method for highly repetitive reference sequences. *BioRxiv*, 2020.11.01.363887. <https://doi.org/10.1101/2020.11.01.363887>
- Jain, C., Rhie, A., Zhang, H., Chu, C., Walenz, B. P., Koren, S., & Phillippy, A. M. (2020). Weighted minimizer sampling improves long read mapping. *Bioinformatics*, 36(Supplement_1), i111–i118. <https://doi.org/10.1093/bioinformatics/btaa435>
- Katoh, K., & Standley, D. M. (2013). MAFFT Multiple Sequence Alignment Software Version 7: Improvements in Performance and Usability. *Molecular Biology and Evolution*, 30(4), 772–780. <https://doi.org/10.1093/molbev/mst010>
- Kim, S., Park, M., Yeom, S.-I., Kim, Y.-M., Lee, J. M., Lee, H.-A., Seo, E., Choi, J., Cheong, K., Kim, K.-T., Jung, K., Lee, G.-W., Oh, S.-K., Bae, C., Kim, S.-B., Lee, H.-Y., Kim, S.-Y., Kim, M.-S., Kang, B.-C., ... Choi, D. (2014). Genome sequence of the hot pepper provides insights into the evolution of pungency in *Capsicum* species. *Nature Genetics*, 46(3), 270–278. <https://doi.org/10.1038/ng.2877>
- Kirsche, M., Prabhu, G., Sherman, R., Ni, B., Aganezov, S., & Schatz, M. C. (2021). Jasmine: Population-scale structural variant comparison and analysis. *BioRxiv*, 2021.05.27.445886. <https://doi.org/10.1101/2021.05.27.445886>
- Kolmogorov, M., Yuan, J., Lin, Y., & Pevzner, P. A. (2019). Assembly of long, error-prone reads using repeat graphs. *Nature Biotechnology*, 37(5), 540–546. <https://doi.org/10.1038/s41587-019-0072-8>

989 Kurtz, S., Phillippy, A., Delcher, A. L., Smoot, M., Shumway, M., Antonescu, C., & Salzberg,
990 S. L. (2004). Versatile and open software for comparing large genomes. *Genome Biology*,
991 5(2), R12. <https://doi.org/10.1186/gb-2004-5-2-r12>

992 Kwon, C.-T., Tang, L., Wang, X., Gentile, I., Hendelman, A., Robitaille, G., Van Eck, J., Xu,
993 C., & Lippman, Z. B. (2022). Dynamic evolution of small signalling peptide compensation
994 in plant stem cell control. *Nature Plants*, 8(4), 346–355. [https://doi.org/10.1038/s41477-](https://doi.org/10.1038/s41477-022-01118-w)
995 022-01118-w

996 Lemmon, Z. H., Reem, N. T., Dalrymple, J., Soyk, S., Swartwood, K. E., Rodriguez-Leal, D.,
997 van Eck, J., & Lippman, Z. B. (2018). Rapid improvement of domestication traits in an
998 orphan crop by genome editing. *Nature Plants*, 4(10), 766–770.
999 <https://doi.org/10.1038/s41477-018-0259-x>

1000 Li, H. (2013). Aligning sequence reads, clone sequences and assembly contigs with BWA-
1001 MEM. *ArXiv: Genomics*.

1002 Li, H. (2018). Minimap2: pairwise alignment for nucleotide sequences. *Bioinformatics*,
1003 34(18), 3094–3100. <https://doi.org/10.1093/bioinformatics/bty191>

1004 Li, H., Handsaker, B., Wysoker, A., Fennell, T., Ruan, J., Homer, N., Marth, G., Abecasis, G.,
1005 Durbin, R., & Subgroup, 1000 Genome Project Data Processing. (2009). The Sequence
1006 Alignment/Map format and SAMtools. *Bioinformatics*, 25(16), 2078–2079.
1007 <https://doi.org/10.1093/bioinformatics/btp352>

1008 Li, J., Song, C., & He, C. (2019). Chinese lantern in *Physalis* is an advantageous
1009 morphological novelty and improves plant fitness. *Scientific Reports*, 9(1), 596.
1010 <https://doi.org/10.1038/s41598-018-36436-7>

1011 Liu, Y., Tikunov, Y., Schouten, R. E., Marcelis, L. F. M., Visser, R. G. F., & Bovy, A. (2018).
1012 Anthocyanin Biosynthesis and Degradation Mechanisms in Solanaceous Vegetables: A
1013 Review. *Frontiers in Chemistry*, 6.
1014 <https://www.frontiersin.org/articles/10.3389/fchem.2018.00052>

1015 Love, M. I., Huber, W., & Anders, S. (2014). Moderated estimation of fold change and
1016 dispersion for RNA-seq data with DESeq2. *Genome Biology*, 15(12), 550.
1017 <https://doi.org/10.1186/s13059-014-0550-8>

1018 Lu, J., Luo, M., Wang, L., Li, K., Yu, Y., Yang, W., Gong, P., Gao, H., Li, Q., Zhao, J., Wu,
1019 L., Zhang, M., Liu, X., Zhang, X., Zhang, X., Kang, J., Yu, T., Li, Z., Jiao, Y., ... He, C.
1020 (2021). The *Physalis floridana* genome provides insights into the biochemical and
1021 morphological evolution of *Physalis* fruits. *Horticulture Research*, 8(1), 244.
1022 <https://doi.org/10.1038/s41438-021-00705-w>

1023 Mapleson, D., Venturini, L., Kaithakottil, G., & Swarbreck, D. (2018). Efficient and accurate
1024 detection of splice junctions from RNA-seq with Portcullis. *GigaScience*, 7(12), giy131.
1025 <https://doi.org/10.1093/gigascience/giy131>

- Marini, F., & Binder, H. (2019). pcaExplorer: an R/Bioconductor package for interacting with RNA-seq principal components. *BMC Bioinformatics*, 20(1), 331. <https://doi.org/10.1186/s12859-019-2879-1>
- Martínez, M. (1993). The correct application of *Physalis pruinosa* L. (Solanaceae). *TAXON*, 42(1), 103–104. <https://doi.org/10.2307/1223312>
- Meir, Z., Aviezer, I., Chongloi, G. L., Ben-Kiki, O., Bronstein, R., Mukamel, Z., Keren-Shaul, H., Jaitin, D., Tal, L., Shalev-Schlosser, G., Harel, T. H., Tanay, A., & Eshed, Y. (2021). Dissection of floral transition by single-meristem transcriptomes at high temporal resolution. *Nature Plants*, 7(6), 800–813. <https://doi.org/10.1038/s41477-021-00936-8>
- Minh, B. Q., Schmidt, H. A., Chernomor, O., Schrempf, D., Woodhams, M. D., von Haeseler, A., & Lanfear, R. (2020). IQ-TREE 2: New Models and Efficient Methods for Phylogenetic Inference in the Genomic Era. *Molecular Biology and Evolution*, 37(5), 1530–1534. <https://doi.org/10.1093/molbev/msaa015>
- Morel, P., Heijmans, K., Rozier, F., Zethof, J., Chamot, S., Bento, S. R., Vialette-Guiraud, A., Chambrier, P., Trehin, C., & Vandenbussche, M. (2017). Divergence of the Floral A-Function between an Asterid and a Rosid Species. *The Plant Cell*, 29(7), 1605–1621. <https://doi.org/10.1105/tpc.17.00098>
- Morgulis, A., Gertz, E. M., Schäffer, A. A., & Agarwala, R. (2006). WindowMasker: window-based masker for sequenced genomes. *Bioinformatics*, 22(2), 134–141. <https://doi.org/10.1093/bioinformatics/bti774>
- Muller, G. B., & Wagner, G. P. (1991). Novelty in Evolution: Restructuring the Concept. *Annual Review of Ecology and Systematics*, 22, 229–256. <http://www.jstor.org/stable/2097261>
- Nurk, S., Walenz, B. P., Rhie, A., Vollger, M. R., Logsdon, G. A., Grothe, R., Miga, K. H., Eichler, E. E., Phillippy, A. M., & Koren, S. (2020). HiCanu: accurate assembly of segmental duplications, satellites, and allelic variants from high-fidelity long reads. *Genome Research*, 30(9), 1291–1305. <https://doi.org/10.1101/gr.263566.120>
- Ou, S., Su, W., Liao, Y., Chougule, K., Agda, J. R. A., Hellinga, A. J., Lugo, C. S. B., Elliott, T. A., Ware, D., Peterson, T., Jiang, N., Hirsch, C. N., & Hufford, M. B. (2019). Benchmarking transposable element annotation methods for creation of a streamlined, comprehensive pipeline. *Genome Biology*, 20(1), 275. <https://doi.org/10.1186/s13059-019-1905-y>
- Padmaja, H., Sruthi, S. R., & Vangalapati, M. (2014). *INTERNATIONAL JOURNAL OF PHARMACY & LIFE SCIENCES (Int. J. of Pharm. Life Sci.) Review on Hibiscus sabdariffa - A valuable herb.*
- Pan, I. L., McQuinn, R., Giovannoni, J. J., & Irish, V. F. (2010). Functional diversification of AGAMOUS lineage genes in regulating tomato flower and fruit development. *Journal of Experimental Botany*, 61(6), 1795–1806. <https://doi.org/10.1093/jxb/erq046>

- Park, S. J., Eshed, Y., & Lippman, Z. B. (2014). Meristem maturation and inflorescence architecture—lessons from the Solanaceae. *Current Opinion in Plant Biology*, 17, 70–77. <https://doi.org/https://doi.org/10.1016/j.pbi.2013.11.006>
- Paton, A. (1990). A Global Taxonomic Investigation of Scutellaria (Labiatae). *Kew Bulletin*, 45(3), 399–450. <https://doi.org/10.2307/4110512>
- Patro, R., Duggal, G., Love, M. I., Irizarry, R. A., & Kingsford, C. (2017). Salmon provides fast and bias-aware quantification of transcript expression. *Nature Methods*, 14(4), 417–419. <https://doi.org/10.1038/nmeth.4197>
- Pertea, G., & Pertea, M. (2020). GFF Utilities: GffRead and GffCompare [version 2; peer review: 3 approved] . *F1000Research*, 9(304). <https://doi.org/10.12688/f1000research.23297.2>
- Pertea, M., Pertea, G. M., Antonescu, C. M., Chang, T.-C., Mendell, J. T., & Salzberg, S. L. (2015). StringTie enables improved reconstruction of a transcriptome from RNA-seq reads. *Nature Biotechnology*, 33(3), 290–295. <https://doi.org/10.1038/nbt.3122>
- Picard toolkit. (2019). In *Broad Institute, GitHub repository*. Broad Institute.
- Pnueli, L., Hareven, D., Rounsley, S. D., Yanofsky, M. F., & Lifschitz, E. (1994). Isolation of the Tomato AGAMOUS Gene TAG1 and Analysis of Its Homeotic Role in Transgenic Plants. *The Plant Cell*, 6(2), 163–173. <https://doi.org/10.2307/3869636>
- Pretz, C., & Deanna, R. (2020). Typifications and nomenclatural notes in *Physalis* (Solanaceae) from the United States. *TAXON*, 69(1), 170–192. <https://doi.org/https://doi.org/10.1002/tax.12159>
- R Core Team. (2020). *R: A Language and Environment for Statistical Computing*. <https://www.R-project.org/>
- Rhie, A., McCarthy, S. A., Fedrigo, O., Damas, J., Formenti, G., Koren, S., Uliano-Silva, M., Chow, W., Functammasan, A., Kim, J., Lee, C., Ko, B. J., Chaisson, M., Gedman, G. L., Cantin, L. J., Thibaud-Nissen, F., Haggerty, L., Bista, I., Smith, M., ... Jarvis, E. D. (2021). Towards complete and error-free genome assemblies of all vertebrate species. *Nature*, 592(7856), 737–746. <https://doi.org/10.1038/s41586-021-03451-0>
- Rhie, A., Walenz, B. P., Koren, S., & Phillippy, A. M. (2020). Merquy: reference-free quality, completeness, and phasing assessment for genome assemblies. *Genome Biology*, 21(1), 245. <https://doi.org/10.1186/s13059-020-02134-9>
- Rydberg, P. A. (1896). The North American species of *Physalis* and related genera. *New York: Torrey Botanical Club*.
- Särkinen, T., Bohs, L., Olmstead, R. G., & Knapp, S. (2013). A phylogenetic framework for evolutionary study of the nightshades (Solanaceae): a dated 1000-tip tree. *BMC Evolutionary Biology*, 13(1), 214. <https://doi.org/10.1186/1471-2148-13-214>

1100 Sato, S., Tabata, S., Hirakawa, H., Asamizu, E., Shirasawa, K., Isobe, S., Kaneko, T.,
1101 Nakamura, Y., Shibata, D., Aoki, K., Egholm, M., Knight, J., Bogden, R., Li, C., Shuang,
1102 Y., Xu, X., Pan, S., Cheng, S., Liu, X., ... Fabra, U. P. (2012). The tomato genome
1103 sequence provides insights into fleshy fruit evolution. *Nature*, 485(7400), 635–641.
1104 <https://doi.org/10.1038/nature11119>

1105 Senthil-Kumar, M., & Mysore, K. S. (2011). Caveat of RNAi in Plants: The Off-Target Effect.
1106 In H. Kodama & A. Komamine (Eds.), *RNAi and Plant Gene Function Analysis: Methods*
1107 *and Protocols* (pp. 13–25). Humana Press. https://doi.org/10.1007/978-1-61779-123-9_2

1108 Shenstone, E., Lippman, Z., & van Eck, J. (2020). A review of nutritional properties and
1109 health benefits of *Physalis* species. *Plant Foods for Human Nutrition*, 75(3), 316–325.
1110 <https://doi.org/10.1007/s11130-020-00821-3>

1111 Shubin, N., Tabin, C., & Carroll, S. (2009). Deep homology and the origins of evolutionary
1112 novelty. *Nature*, 457(7231), 818–823. <https://doi.org/10.1038/nature07891>

1113 Shumate, A., & Salzberg, S. L. (2021). Liftoff: accurate mapping of gene annotations.
1114 *Bioinformatics*, 37(12), 1639–1643. <https://doi.org/10.1093/bioinformatics/btaa1016>

1115 Simão, F. A., Waterhouse, R. M., Ioannidis, P., Kriventseva, E. v., & Zdobnov, E. M. (2015).
1116 BUSCO: assessing genome assembly and annotation completeness with single-copy
1117 orthologs. *Bioinformatics*, 31(19), 3210–3212.
1118 <https://doi.org/10.1093/bioinformatics/btv351>

1119 Sonesson, C., Love, M. I., & Robinson, M. D. (2016). Differential analyses for RNA-seq:
1120 transcript-level estimates improve gene-level inferences [version 2; peer review: 2
1121 approved] . *F1000Research*, 4(1521). <https://doi.org/10.12688/f1000research.7563.2>

1122 Soyk, S., Lemmon, Z. H., Oved, M., Fisher, J., Liberatore, K. L., Park, S. J., Goren, A., Jiang,
1123 K., Ramos, A., van der Knaap, E., van Eck, J., Zamir, D., Eshed, Y., & Lippman, Z. B.
1124 (2017). Bypassing Negative Epistasis on Yield in Tomato Imposed by a Domestication
1125 Gene. *Cell*, 169(6), 1142–1155.e12. <https://doi.org/10.1016/j.cell.2017.04.032>

1126 Spelt, C., Quattrocchio, F., Mol, J., & Koes, R. (2002). ANTHOCYANIN1 of *Petunia*
1127 Controls Pigment Synthesis, Vacuolar pH, and Seed Coat Development by Genetically
1128 Distinct Mechanisms. *The Plant Cell*, 14(9), 2121–2135.
1129 <https://doi.org/10.1105/tpc.003772>

1130 Spelt, C., Quattrocchio, F., Mol, J. N. M., & Koes, R. (2000). anthocyanin1 of *Petunia*
1131 Encodes a Basic Helix-Loop-Helix Protein That Directly Activates Transcription of
1132 Structural Anthocyanin Genes. *The Plant Cell*, 12(9), 1619–1631.
1133 <https://doi.org/10.1105/tpc.12.9.1619>

1134 Sugiyama, Y., Watase, Y., Nagase, M., Makita, N., Yagura, S., Hirai, A., & Sugiura, M.
1135 (2005). The complete nucleotide sequence and multipartite organization of the tobacco
1136 mitochondrial genome: comparative analysis of mitochondrial genomes in higher plants.

1137 *Molecular Genetics and Genomics*, 272(6), 603–615. <https://doi.org/10.1007/s00438-004->
1138 1075-8

1139 Swartwood, K., & van Eck, J. (2019). Development of plant regeneration and *Agrobacterium*
1140 tumefaciens-mediated transformation methodology for *Physalis pruinosa*. *Plant Cell,*
1141 *Tissue and Organ Culture (PCTOC)*, 137(3), 465–472. <https://doi.org/10.1007/s11240->
1142 019-01582-x

1143 Takagi, H., Abe, A., Yoshida, K., Kosugi, S., Natsume, S., Mitsuoka, C., Uemura, A., Utsushi,
1144 H., Tamiru, M., Takuno, S., Innan, H., Cano, L. M., Kamoun, S., & Terauchi, R. (2013).
1145 QTL-seq: rapid mapping of quantitative trait loci in rice by whole genome resequencing of
1146 DNA from two bulked populations. *The Plant Journal*, 74(1), 174–183.
1147 <https://doi.org/https://doi.org/10.1111/tpj.12105>

1148 Tamura, K., Stecher, G., & Kumar, S. (2021). MEGA11: Molecular Evolutionary Genetics
1149 Analysis Version 11. *Molecular Biology and Evolution*, 38(7), 3022–3027.
1150 <https://doi.org/10.1093/molbev/msab120>

1151 Theißen, G., & Saedler, H. (2001). Floral quartets. *Nature*, 409(6819), 469–471.
1152 <https://doi.org/10.1038/35054172>

1153 Venturini, L., Caim, S., Kaithakottil, G. G., Mapleson, D. L., & Swarbreck, D. (2018).
1154 Leveraging multiple transcriptome assembly methods for improved gene structure
1155 annotation. *GigaScience*, 7(8), giy093. <https://doi.org/10.1093/gigascience/giy093>

1156 Waterfall, U. T. (1967). PHYSALIS IN MEXICO, CENTRAL AMERICA AND THE WEST
1157 INDIES. *Rhodora*, 69(777), 82–120. <http://www.jstor.org/stable/23311644>

1158 Waterfall, U. T. (Urnaldy T. (1958). A taxonomic study of the genus *Physalis* in North
1159 America north of Mexico. *Rhodora*, 60, 152–173.
1160 <https://www.biodiversitylibrary.org/part/124500>

1161 Wei, Q., Wang, J., Wang, W., Hu, T., Hu, H., & Bao, C. (2020). A high-quality chromosome-
1162 level genome assembly reveals genetics for important traits in eggplant. *Horticulture*
1163 *Research*, 7(1), 153. <https://doi.org/10.1038/s41438-020-00391-0>

1164 Weigel, D., & Meyerowitz, E. M. (1994). The ABCs of floral homeotic genes. *Cell*, 78(2),
1165 203–209. [https://doi.org/https://doi.org/10.1016/0092-8674\(94\)90291-7](https://doi.org/https://doi.org/10.1016/0092-8674(94)90291-7)

1166 Whitson, M. (2012). CALLIPHYSALIS (SOLANACEAE): A NEW GENUS FROM THE
1167 SOUTHEASTERN USA. *Rhodora*, 114(958), 133–147.
1168 <http://www.jstor.org/stable/23314732>

1169 Wilf, P., Carvalho, M. R., Gandolfo, M. A., & Cúneo, N. R. (2017). Eocene lantern fruits from
1170 Gondwanan Patagonia and the early origins of Solanaceae. *Science*, 355(6320), 71–75.
1171 <https://doi.org/10.1126/science.aag2737>

1172 Xu, P., Zhang, Y., Kang, L., Roossinck, M. J., & Mysore, K. S. (2006). Computational
1173 Estimation and Experimental Verification of Off-Target Silencing during

1174 Posttranscriptional Gene Silencing in Plants. *Plant Physiology*, 142(2), 429–440.
1175 <https://doi.org/10.1104/pp.106.083295>

1176 Xu, X., Pan, S., Cheng, S., Zhang, B., Mu, D., Ni, P., Zhang, G., Yang, S., Li, R., Wang, J.,
1177 Orjeda, G., Guzman, F., Torres, M., Lozano, R., Ponce, O., Martinez, D., de la Cruz, G.,
1178 Chakrabarti, S. K., Patil, V. U., ... Centre, W. U. & R. (2011). Genome sequence and
1179 analysis of the tuber crop potato. *Nature*, 475(7355), 189–195.
1180 <https://doi.org/10.1038/nature10158>

1181 Yanofsky, M. F., Ma, H., Bowman, J. L., Drews, G. N., Feldmann, K. A., & Meyerowitz, E.
1182 M. (1990). The protein encoded by the Arabidopsis homeotic gene *agamous* resembles
1183 transcription factors. *Nature*, 346(6279), 35–39. <https://doi.org/10.1038/346035a0>

1184 Yuste-Lisbona, F. J., Quinet, M., Fernández-Lozano, A., Pineda, B., Moreno, V., Angosto, T.,
1185 & Lozano, R. (2016). Characterization of vegetative inflorescence (*mc-vin*) mutant
1186 provides new insight into the role of MACROCALYX in regulating inflorescence
1187 development of tomato. *Scientific Reports*, 6(1), 18796. <https://doi.org/10.1038/srep18796>

1188 Zamora-Tavares, M. del P., Martínez, M., Magallón, S., Guzmán-Dávalos, L., & Vargas-
1189 Ponce, O. (2016). *Physalis* and *physaloids*: A recent and complex evolutionary history.
1190 *Molecular Phylogenetics and Evolution*, 100, 41–50.
1191 <https://doi.org/https://doi.org/10.1016/j.ympev.2016.03.032>

1192 Zhang, J.-S., Li, Z., Zhao, J., Zhang, S., Quan, H., Zhao, M., & He, C. (2014). Deciphering the
1193 *Physalis floridana* Double-Layered-Lantern1 Mutant Provides Insights into Functional
1194 Divergence of the GLOBOSA Duplicates within the Solanaceae . *Plant Physiology*,
1195 164(2), 748–764. <https://doi.org/10.1104/pp.113.233072>

1196 Zhang, W.-N., & Tong, W.-Y. (2016). Chemical Constituents and Biological Activities of
1197 Plants from the Genus *Physalis*. *Chemistry & Biodiversity*, 13(1), 48–65.
1198 <https://doi.org/https://doi.org/10.1002/cbdv.201400435>

1199 Zhao, J., Tian, Y., Zhang, J.-S., Zhao, M., Gong, P., Riss, S., Saedler, R., & He, C. (2013). The
1200 euAP1 protein MPF3 represses MPF2 to specify floral calyx identity and displays crucial
1201 roles in Chinese lantern development in *Physalis*. *The Plant Cell*, 25(6), 2002–2021.
1202 <https://doi.org/10.1105/tpc.113.111757>

1203

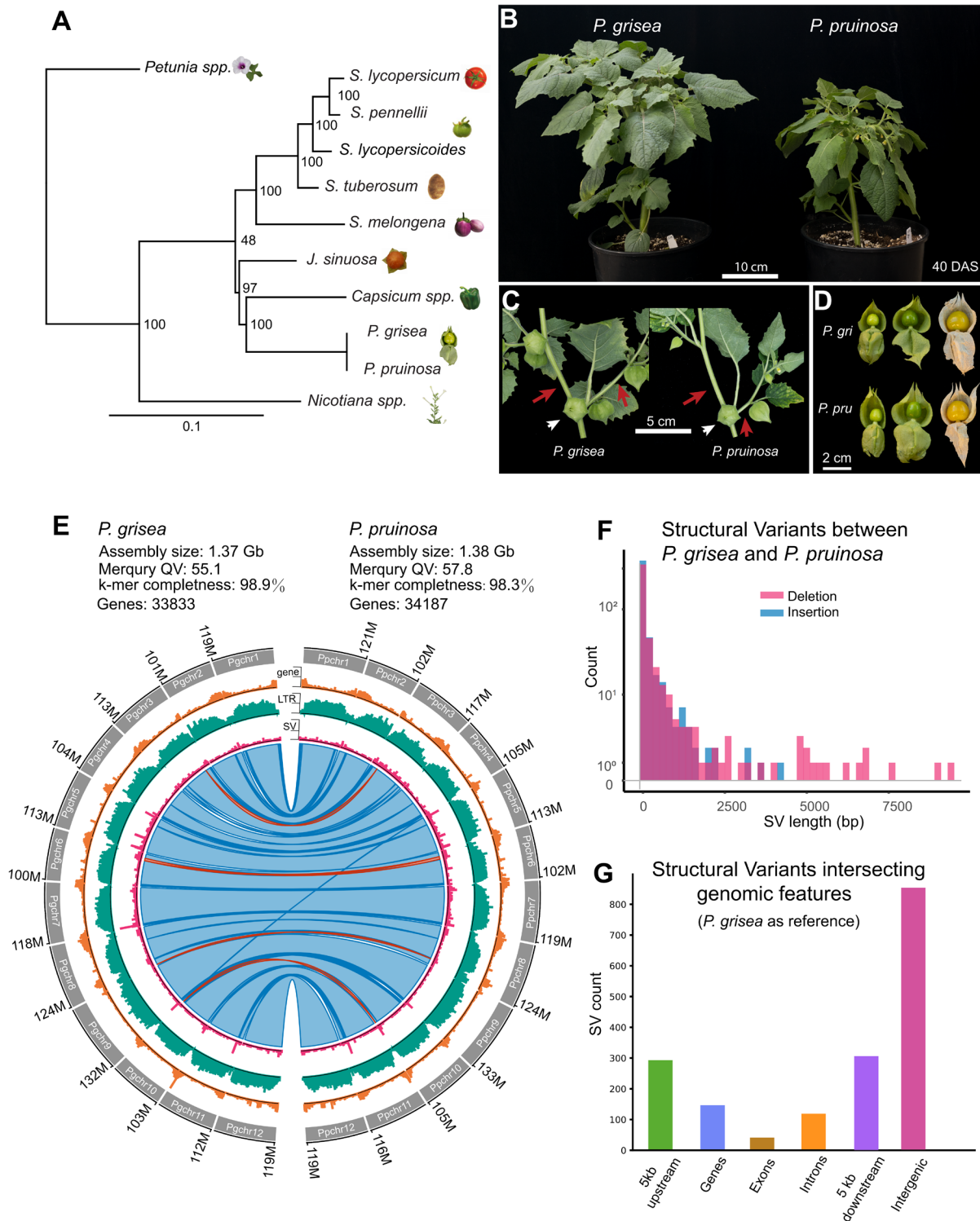


Figure 1. Reference-quality genome assemblies of *P. grisea* and *P. pruinosa*.

A. Phylogeny of selected *Solanaceae* species based on the 20 most conserved protein sequences (see **Methods**). **B.** Whole plant images of *P. grisea* and *P. pruinosa* 40 d after sowing (DAS) in greenhouse conditions. Bar = 10 cm. **C.**

Sympodial shoot architectures of *P. grisea* and *P. pruinosa*. Quantification of internode lengths is in **Supplemental Data Set S1**. Bar = 5 cm. **D.** Images of *P. grisea* and *P. pruinosa* calyces and fruits at different stages of development. Husks were manually opened to show fruits. Bar = 2 cm. **E.** Circos plots comparing *P. grisea* and *P. pruinosa* genomes. Circos quantitative tracks are summed in 100-kbp windows and show the number of genes (lower tick = 0, middle tick = 25, higher tick = 49), LTR retrotransposons (lower tick = 0, middle tick = 102, higher tick = 204) and SVs (lower tick = 0, middle tick = 4, higher tick = 9). The inner ribbon track shows whole genome alignments, with blue indicating forward-strand alignments and red indicating reverse-strand alignments (inversions). Darker colors indicate alignment boundaries. **F.** Distribution of deletion and insertion SVs between 30 bp and 10 kbp from *P. pruinosa* compared to *P. grisea*, summed in 200-bp windows. **G.** Counts of SVs intersecting genomic features, comparing *P. pruinosa* to *P. grisea*.

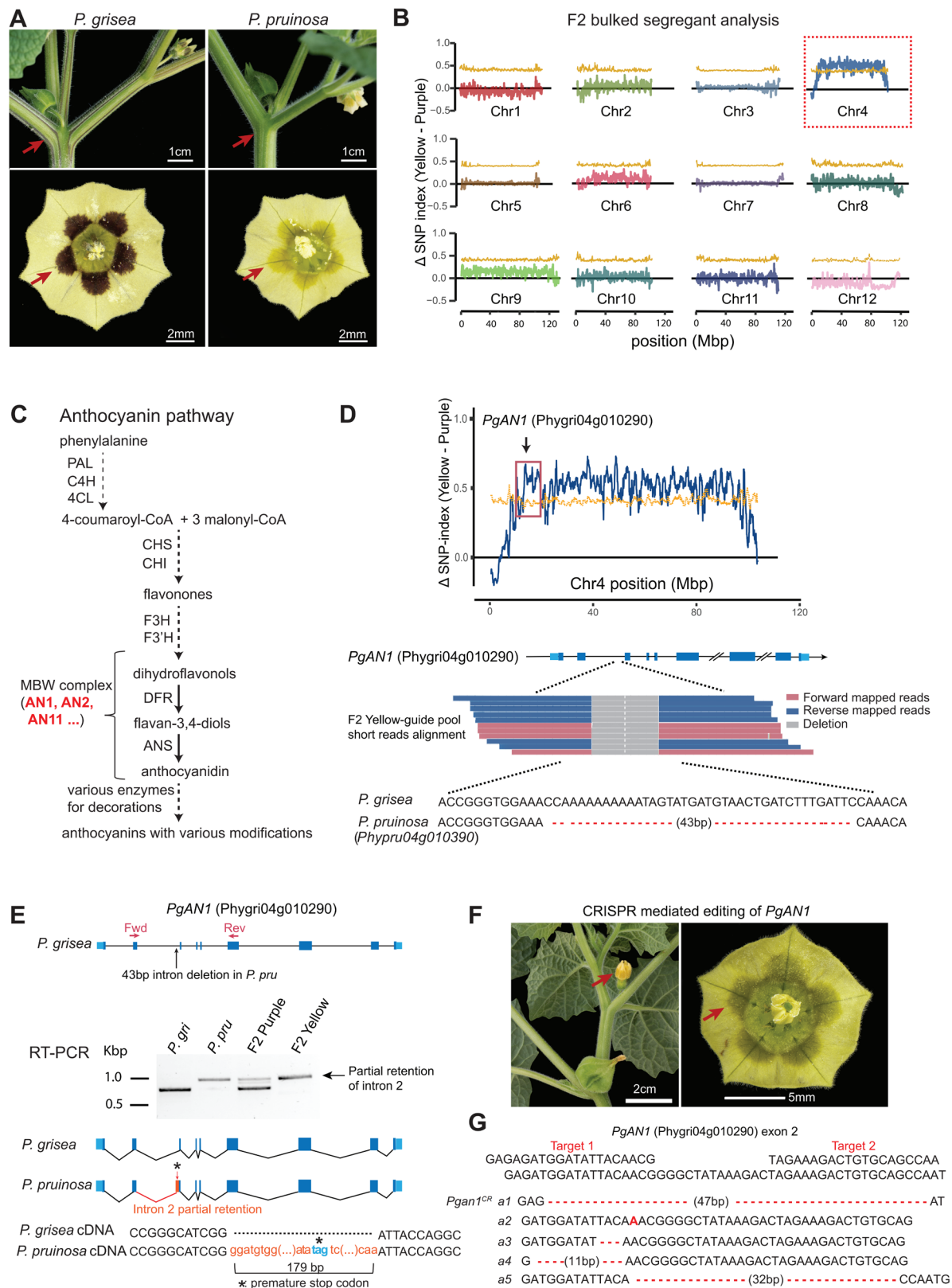


Figure 2. Loss of purple pigmentation in *P. pruinosa* is due to an intronic SV in the bHLH transcription factor gene *ANTHOCYANIN1*.

A. Images showing the difference in pigmentation between *P. grisea* and *P. pruinosa*. Arrows point to purple (*P. grisea*) compared to yellow (*P. pruinosa*) pigmentation on stems and flowers. Top bars = 1 cm; bottom bars = 2 mm. **B.** Mapping by sequencing showing the Δ SNP-index across all twelve chromosomes using *P. grisea* as the reference, with SNP ratios between yellow-guide and the purple-guide pools from an interspecific F2 population. Yellow line: 95% confidence interval cut-offs of Δ SNP-index. **C.** Simplified pathway of anthocyanin biosynthesis based on data from petunia. Major transcriptional and enzymatic regulators are shown as abbreviations. PAL: Phenylalanine Ammonialyase; C4H: Cinnamate 4-Hydroxylase; 4CL: 4-Coumaroyl-CoA ligase; CHS: Chalcone Synthase; CHI: Chalcone Isomerase; F3H: Flavanone 3-hydroxylase; F3'H: Flavonoid 3'-hydroxylase; AN1: ANTHOCYANIN 1; AN2: ANTHOCYANIN 2; AN11: ANTHOCYANIN 11; DFR: Dihydroflavonol Reductase; ANS: Anthocyanin Synthase. Dashed lines indicate multiple steps condensed. Bold red font indicates components of the MYB-bHLH-WD40 (MBW) complex that transcriptionally activates late biosynthetic genes. **D.** Top: The Δ SNP-index plot for chromosome 4. The black arrow points to the genomic location of the *AN1* candidate gene. Bottom: a composite of Illumina mapped-reads from *P. pruinosa* at the 2nd intron of *AN1* showing a 43-bp deletion in all *PpAN1* (*Phypru04g010390*) sequences. In all gene models (including later figures), deep blue boxes, black lines, and light blue boxes represent exonic, intronic, and untranslated regions, respectively. **E.** Molecular consequences of the 43-bp intronic deletion in *PpAN1* revealed by RT-PCR and sequencing. Red arrows indicate the forward and reverse RT-PCR primers. Longer amplicons and thus *AN1* transcripts from both the yellow-guide F2 bulk pool and *P. pruinosa* were identified by agarose gel electrophoresis. Sanger sequencing revealed the inclusion of a 179-bp fragment of intron 2 in the *PpAN1* amplicon, resulting in a premature stop codon. Red box reflects intronic sequence retained in the transcript. Black asterisk, premature stop. **F.** Loss of purple pigmentation in CRISPR edited *PgAN1* T₀ plants. Left bar = 2 cm; right bar = 5 mm. **G.** CRISPR-Cas9 generated mutant alleles from the yellow T₀ chimeric plants are shown. Red dashed lines represent deletions. The red bold letter indicates a single nucleotide insertion.

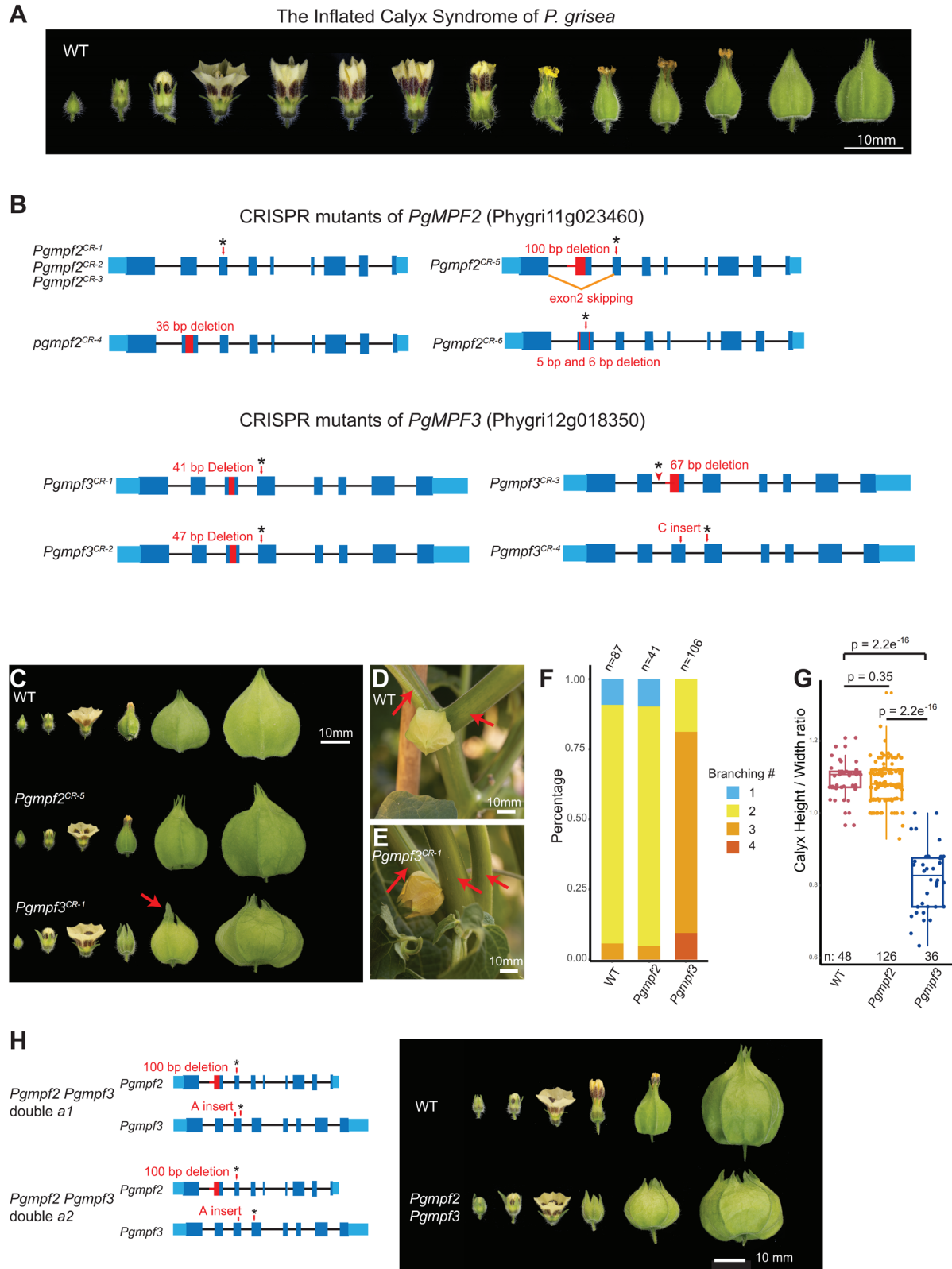


Figure 3. CRISPR-Cas9 generated mutants of the MADS-box genes *PgMPF2* and *PgMPF3* do not prevent ICS.
A. Images showing sequential stages of ICS in *P. grisea* from early flower formation to calyx inflation over 3 d. Bar = 10 mm. **B.** Multiple, independently derived null alleles in *PgMPF2* and *PgMPF3*. Red boxes and lines, deletions; black

asterisks, stop codons. Three alleles of *PgMPF2* (*Pgmpf2^{CR-1}*, *Pgmpf2^{CR-2}*, *Pgmpf2^{CR-3}*) with different mutations in exon 3 result in the same premature stop codon. Specific mutations for all alleles are shown in **Supplemental Figure S2** and in **Supplemental Data Set S3**. **C-G**. Phenotypes of *Pgmpf2* and *Pgmpf3* null mutants. All homozygous mutants independently derived alleles showed the same phenotypes, and *Pgmpf2^{CR-5}* and *Pgmpf3^{CR-1}* were used as references for phenotypic analyses. **C**. Calyx inflation is not disrupted in *Pgmpf2* and *Pgmpf3* mutants. Representative images from *Pgmpf2^{CR-5}* and *Pgmpf3^{CR-1}* are shown. The leaf-like sepal tip of *Pgmpf3^{CR-1}* is indicated by the red arrow. Bar = 10 mm. **D** and **E**. Shoot branching phenotype of *Pgmpf3^{CR-1}* compared to WT. A typical sympodial unit of WT *Physalis* consists of one leaf, one flower and two side shoots. *Pgmpf3* mutants develop mostly three side shoots. Bar = 10 mm. **(E)**. Branches are indicated by red arrows in representative images. **F**. Quantification of branching in WT, *Pgmpf2* and *Pgmpf3* shown as stacked bar charts. Branching counts are shown in **Supplemental Data Set S4**. **G**. Quantification of calyx height/width ratio in WT, *Pgmpf2* and *Pgmpf3*. Raw measurements are shown in **Supplemental Data Set S5**. Statistical significance determined by two-tailed, two-sample *t*-tests, and *p* values are shown. **H**. Calyx inflation is not disrupted in *Pgmpf2 Pgmpf3* double mutants. Two allelic combinations in double mutants of *Pgmpf2 Pgmpf3* (*a1* and *a2*) displayed the same phenotype, and allele *a2* was used as reference in the image shown. Bar = 10 mm.

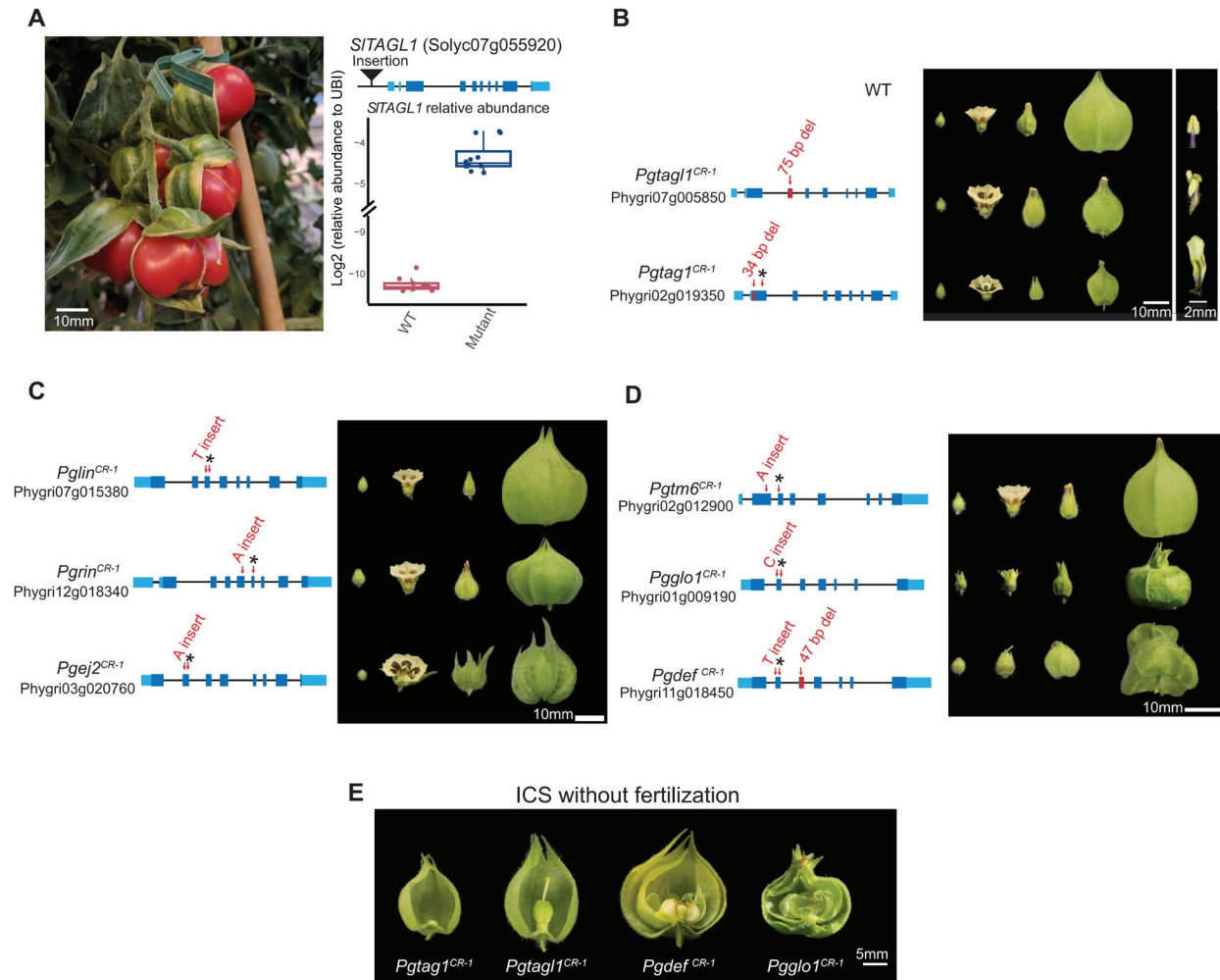


Figure 4. CRISPR-Cas9 generated mutations in eight additional candidate MADS-box genes do not disrupt ICS.

A. Overexpression of *SITAGL1* caused by a transposable element insertion (see **Methods**) results in an enlarged calyx in tomato, mimicking ICS and presenting another candidate MADS-box gene. Left: image of calyx phenotype from the *SITAGL1* mutant. Bar = 10 mm. Right, top: gene model of *SITAGL1* with the transposon insertion (black triangle) identified by genome sequencing. Right, bottom: RT-qPCR on cDNA derived from young sepals showing overexpression of *SITAGL1* in the mutant. Sepal tissue from three WT plants, and from four mutant plants were assayed (see **methods**); each data point represents one technical replicate. **B.** Mutations in *PgTAGL1* and *PgTAG1* cause homeotic transformations of stamens to petal-like organs but do not disrupt ICS. Middle image: representative calyx phenotypes at different developmental stages. Bar = 10 mm. Right image: single organs from the 3rd floral whorl. Bar = 2 mm. **C.** Mutations in three *SEP4* homologs do not disrupt ICS. Bar = 10 mm. **D.** Mutations in multiple B-function MADS-box genes do not disrupt ICS. Bar = 10 mm. **E.** ICS still occurs in mutants with fertilization defects or those that fail to produce fruits. Mutations in *PgTAG1*, *PgTAGL1*, *PgDEF*, and *PgGLO1* cause homeotic transformations of floral organs that abolish self-fertilization, but ICS is preserved. Bar = 5 mm.

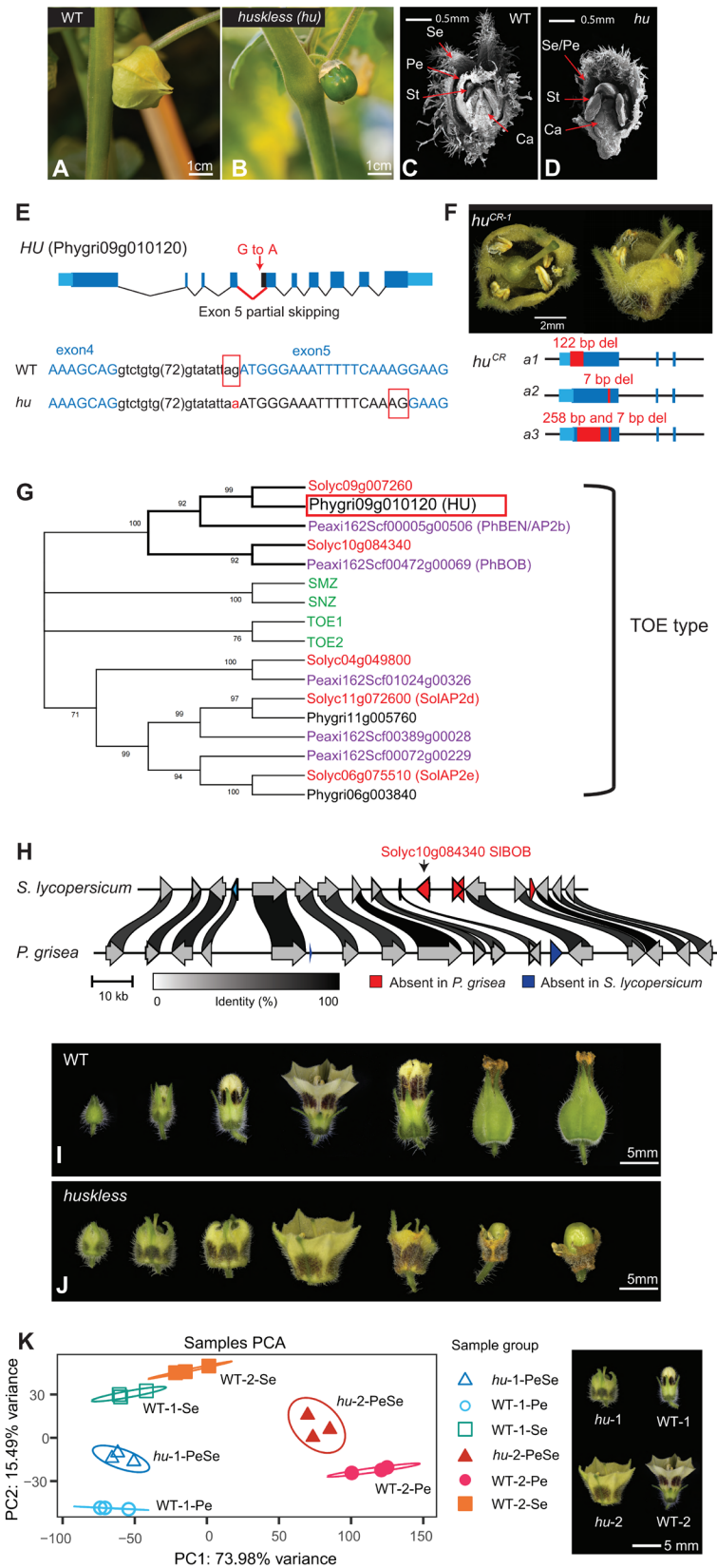


Figure 5. The *huskless* mutant lacks an inflated calyx due to mutation of an AP2-like transcription factor. A-D. Phenotypes of the EMS-derived *huskless (hu)* mutant. **A** and **B**. Images of WT and the *hu* mutant displaying the loss

of calyx phenotype at the mature green fruit stage. Bar = 1 cm. **C** and **D**. Longitudinal SEM images of developing flowers of WT and *hu* showing *hu* mutants develop only three floral whorls compared to four in WT. The first whorl of *hu* flowers shows hallmarks of sepal and petal identity. Se: sepal; Pe: petal; St: stamen; Ca: Carpel. Bar = 0.5 mm. **E**. Gene model showing the G-to-A point mutation causing partial skipping of exon 5 in the *AP2-like* transcription factor gene *Phygri09g010120*. Blue-colored nucleotides represent exonic sequences; red boxes indicate 3' splice sites in WT and *hu*. **F**. CRISPR-Cas9 generated mutations in *Phygri09g010120*. Top: gene models showing three independent CRISPR null alleles of *hu*. Sequences 3' of the 3rd intron are omitted. *hu^{CR-1}* is homozygous for allele 1 (*a1*). Bottom: images of *hu^{CR-1}* flower phenotype. Bar = 2 mm. **G**. Maximum likelihood consensus tree of the TOE-type euAP2 proteins from *A. thaliana* (gene names in green), *P. axillaris* (Peaxi IDs in purple), *S. lycopersicum* (Solyc IDs in red), and *P. grisea* (Phygri IDs in black). Bootstrap values (%) based on 500 replicates are indicated near the branching points; branches below 50% have been collapsed. **H**. Local synteny analysis between *S. lycopersicum* and *P. grisea* showing the absence of the *Solyc10g084340* orthologue (petunia *BOB* orthologue) in *P. grisea*. Arrows indicate genes and orientations. Protein identity percentages between orthologues are indicated by ribbon shades in grayscale; only links above 80% identity are shown. **I** and **J**. Series of images of WT and *hu* developing flowers from before anthesis through early fruit development. Bar = 5 mm. **K**. Principal component analysis (PCA) of WT and *hu* RNA-seq data. Right image: visual reference of the two stages used for expression profiling from WT and *hu* floral whorls. Numbers (-1 or -2) in the sample groups represent stage 1 or 2; petal or sepal whorls in WT are denoted as Pe, Se respectively; PeSe represents the merged outer whorl in *hu*. The top 3000 differentially expressed genes were used for PCA. Bar = 5 mm.

Parsed Citations

- Alonge, M., Lebeigle, L., Kirsche, M., Aganezov, S., Wang, X., Lippman, Z. B., Schatz, M. C., & Soyk, S. (2021). Automated assembly scaffolding elevates a new tomato system for high-throughput genome editing. *BioRxiv*, 2021.11.18.469135. <https://doi.org/10.1101/2021.11.18.469135>
Google Scholar: [Author Only](#) [Title Only](#) [Author and Title](#)
- Alonge, M., Wang, X., Benoit, M., Soyk, S., Pereira, L., Zhang, L., Suresh, H., Ramakrishnan, S., Maumus, F., Ciren, D., Levy, Y., Harel, T. H., Shalev-Schlosser, G., Amsellem, Z., Razifard, H., Caicedo, A. L., Tieman, D. M., Klee, H., Kirsche, M., ... Lippman, Z. B. (2020). Major Impacts of Widespread Structural Variation on Gene Expression and Crop Improvement in Tomato. *Cell*, 182(1), 145-161.e23. <https://doi.org/https://doi.org/10.1016/j.cell.2020.05.021>
Google Scholar: [Author Only](#) [Title Only](#) [Author and Title](#)
- Altschul, S. F., Gish, W., Miller, W., Myers, E. W., & Lipman, D. J. (1990). Basic local alignment search tool. *Journal of Molecular Biology*, 215(3), 403–410. [https://doi.org/https://doi.org/10.1016/S0022-2836\(05\)80360-2](https://doi.org/https://doi.org/10.1016/S0022-2836(05)80360-2)
Google Scholar: [Author Only](#) [Title Only](#) [Author and Title](#)
- Añibarro-Ortega, M., Pinela, J., Alexopoulos, A., Petropoulos, S. A., Ferreira, I. C. F. R., & Barros, L. (2022). Chapter Four - The powerful Solanaceae: Food and nutraceutical applications in a sustainable world. In F. Toldrá (Ed.), *Advances in Food and Nutrition Research* (Vol. 100, pp. 131–172). Academic Press. <https://doi.org/https://doi.org/10.1016/bs.afnr.2022.03.004>
Google Scholar: [Author Only](#) [Title Only](#) [Author and Title](#)
- Bairoch, A., & Apweiler, R. (2000). The SWISS-PROT protein sequence database and its supplement TrEMBL in 2000. *Nucleic Acids Research*, 28(1), 45–48. <https://doi.org/10.1093/nar/28.1.45>
Google Scholar: [Author Only](#) [Title Only](#) [Author and Title](#)
- Baumann, T. W., & Meier, C. M. (1993). Chemical defence by withanolides during fruit development in *Physalis peruviana*. *Phytochemistry*, 33(2), 317–321. [https://doi.org/https://doi.org/10.1016/0031-9422\(93\)85510-X](https://doi.org/https://doi.org/10.1016/0031-9422(93)85510-X)
Google Scholar: [Author Only](#) [Title Only](#) [Author and Title](#)
- Bolger, A. M., Lohse, M., & Usadel, B. (2014). Trimmomatic: a flexible trimmer for Illumina sequence data. *Bioinformatics*, 30(15), 2114–2120. <https://doi.org/10.1093/bioinformatics/btu170>
Google Scholar: [Author Only](#) [Title Only](#) [Author and Title](#)
- Bombarely, A., Moser, M., Amrad, A., Bao, M., Bapaume, L., Barry, C. S., Bliet, M., Boersma, M. R., Borghi, L., Bruggmann, R., Bucher, M., D'Agostino, N., Davies, K., Druege, U., Dudareva, N., Egea-Cortines, M., Delledonne, M., Fernandez-Pozo, N., Franken, P., ... Kuhlemeier, C. (2016). Insight into the evolution of the Solanaceae from the parental genomes of *Petunia hybrida*. *Nature Plants*, 2(6), 16074. <https://doi.org/10.1038/nplants.2016.74>
Google Scholar: [Author Only](#) [Title Only](#) [Author and Title](#)
- Chang, C., Bowman, J. L., & Meyerowitz, E. M. (2016). Field Guide to Plant Model Systems. *Cell*, 167(2), 325–339. <https://doi.org/https://doi.org/10.1016/j.cell.2016.08.031>
Google Scholar: [Author Only](#) [Title Only](#) [Author and Title](#)
- Cheng, H., Concepcion, G. T., Feng, X., Zhang, H., & Li, H. (2021). Haplotype-resolved de novo assembly using phased assembly graphs with hifiasm. *Nature Methods*, 18(2), 170–175. <https://doi.org/10.1038/s41592-020-01056-5>
Google Scholar: [Author Only](#) [Title Only](#) [Author and Title](#)
- Cingolani, P., Platts, A., Wang, L. L., Coon, M., Nguyen, T., Wang, L., Land, S. J., Lu, X., & Ruden, D. M. (2012). A program for annotating and predicting the effects of single nucleotide polymorphisms, SnpEff. *Fly*, 6(2), 80–92. <https://doi.org/10.4161/fly.19695>
Google Scholar: [Author Only](#) [Title Only](#) [Author and Title](#)
- Danecek, P., Auton, A., Abecasis, G., Albers, C. A., Banks, E., DePristo, M. A., Handsaker, R. E., Lunter, G., Marth, G. T., Sherry, S. T., McVean, G., Durbin, R., & Group, 1000 Genomes Project Analysis. (2011). The variant call format and VCFtools. *Bioinformatics*, 27(15), 2156–2158. <https://doi.org/10.1093/bioinformatics/btr330>
Google Scholar: [Author Only](#) [Title Only](#) [Author and Title](#)
- Danecek, P., Bonfield, J. K., Liddle, J., Marshall, J., Ohan, V., Pollard, M. O., Whitwham, A., Keane, T., McCarthy, S. A., Davies, R. M., & Li, H. (2021). Twelve years of SAMtools and BCFtools. *GigaScience*, 10(2), giab008. <https://doi.org/10.1093/gigascience/giab008>
Google Scholar: [Author Only](#) [Title Only](#) [Author and Title](#)
- Deanna, R., Larter, M. D., Barboza, G. E., & Smith, S. D. (2019). Repeated evolution of a morphological novelty: a phylogenetic analysis of the inflated fruiting calyx in the Physalideae tribe (Solanaceae). *American Journal of Botany*, 106(2), 270–279. <https://doi.org/https://doi.org/10.1002/ajb2.1242>
Google Scholar: [Author Only](#) [Title Only](#) [Author and Title](#)
- Deanna, R., Wilf, P., & Gandolfo, M. A. (2020). New physaloid fruit-fossil species from early Eocene South America. *American Journal of Botany*, 107(12), 1749–1762. <https://doi.org/https://doi.org/10.1002/ajb2.1565>
Google Scholar: [Author Only](#) [Title Only](#) [Author and Title](#)

Dobin, A., Davis, C. A., Schlesinger, F., Drenkow, J., Zaleski, C., Jha, S., Batut, P., Chaisson, M., & Gingeras, T. R. (2013). STAR: ultrafast universal RNA-seq aligner. *Bioinformatics*, 29(1), 15–21. <https://doi.org/10.1093/bioinformatics/bts635>

Google Scholar: [Author Only](#) [Title Only](#) [Author and Title](#)

Dudchenko, O., Shamim, M. S., Batra, S. S., Durand, N. C., Musial, N. T., Mostofa, R., Pham, M., Glenn St Hilaire, B., Yao, W., Stamenova, E., Hoeger, M., Nyquist, S. K., Korchina, V., Pletch, K., Flanagan, J. P., Tomaszewicz, A., McAloose, D., Pérez Estrada, C., Novak, B. J., ... Aiden, E. L. (2018). The Juicebox Assembly Tools module facilitates *de novo* assembly of mammalian genomes with chromosome-length scaffolds for under \$1000. *BioRxiv*, 254797. <https://doi.org/10.1101/254797>

Google Scholar: [Author Only](#) [Title Only](#) [Author and Title](#)

FastQC. (2015). <https://qubeshub.org/resources/fastqc>

Gao, H., Li, J., Wang, L., Zhang, J., & He, C. (2020). Transcriptomic variation of the flower–fruit transition in *Physalis* and *Solanum*. *Planta*, 252(2), 28. <https://doi.org/10.1007/s00425-020-03434-x>

Google Scholar: [Author Only](#) [Title Only](#) [Author and Title](#)

Gao, L., Gonda, I., Sun, H., Ma, Q., Bao, K., Tieman, D. M., Burzynski-Chang, E. A., Fish, T. L., Stromberg, K. A., Sacks, G. L., Thannhauser, T. W., Foolad, M. R., Diez, M. J., Blanca, J., Canizares, J., Xu, Y., van der Knaap, E., Huang, S., Klee, H. J., ... Fei, Z. (2019). The tomato pan-genome uncovers new genes and a rare allele regulating fruit flavor. *Nature Genetics*, 51(6), 1044–1051. <https://doi.org/10.1038/s41588-019-0410-2>

Google Scholar: [Author Only](#) [Title Only](#) [Author and Title](#)

Garrison, E. P., & Marth, G. T. (2012). Haplotype-based variant detection from short-read sequencing. *ArXiv: Genomics*.

Google Scholar: [Author Only](#) [Title Only](#) [Author and Title](#)

Gebhardt, C. (2016). The historical role of species from the Solanaceae plant family in genetic research. *Theoretical and Applied Genetics*, 129(12), 2281–2294. <https://doi.org/10.1007/s00122-016-2804-1>

Google Scholar: [Author Only](#) [Title Only](#) [Author and Title](#)

Gilchrist, C. L. M., & Chooi, Y.-H. (2021). clinker & clustermap.js: automatic generation of gene cluster comparison figures. *Bioinformatics*, 37(16), 2473–2475. <https://doi.org/10.1093/bioinformatics/btab007>

Google Scholar: [Author Only](#) [Title Only](#) [Author and Title](#)

Grandillo, S., & Tanksley, S. D. (1996). QTL analysis of horticultural traits differentiating the cultivated tomato from the closely related species *Lycopersicon pimpinellifolium*. *Theoretical and Applied Genetics*, 92(8), 935–951. <https://doi.org/10.1007/BF00224033>

Google Scholar: [Author Only](#) [Title Only](#) [Author and Title](#)

Guan, D., McCarthy, S. A., Wood, J., Howe, K., Wang, Y., & Durbin, R. (2020). Identifying and removing haplotypic duplication in primary genome assemblies. *Bioinformatics*, 36(9), 2896–2898. <https://doi.org/10.1093/bioinformatics/btaa025>

Google Scholar: [Author Only](#) [Title Only](#) [Author and Title](#)

He, C., Münster, T., & Saedler, H. (2004). On the origin of floral morphological novelties. *FEBS Letters*, 567(1), 147–151. <https://doi.org/https://doi.org/10.1016/j.febslet.2004.02.090>

Google Scholar: [Author Only](#) [Title Only](#) [Author and Title](#)

He, C., & Saedler, H. (2005). Heterotopic expression of MPF2 is the key to the evolution of the Chinese lantern of *Physalis*, a morphological novelty in Solanaceae. *Proceedings of the National Academy of Sciences of the United States of America*, 102(16), 5779–5784. <https://doi.org/10.1073/pnas.0501877102>

Google Scholar: [Author Only](#) [Title Only](#) [Author and Title](#)

He, C., & Saedler, H. (2007). Hormonal control of the inflated calyx syndrome, a morphological novelty, in *Physalis*. *The Plant Journal*, 49(5), 935–946. <https://doi.org/https://doi.org/10.1111/j.1365-313X.2006.03008.x>

Google Scholar: [Author Only](#) [Title Only](#) [Author and Title](#)

Hendelman, A., Zebell, S., Rodriguez-Leal, D., Dukler, N., Robitaille, G., Wu, X., Kostyun, J., Tal, L., Wang, P., Bartlett, M. E., Eshed, Y., Efroni, I., & Lippman, Z. B. (2021). Conserved pleiotropy of an ancient plant homeobox gene uncovered by cis-regulatory dissection. *Cell*, 184(7), 1724–1739.e16. <https://doi.org/https://doi.org/10.1016/j.cell.2021.02.001>

Google Scholar: [Author Only](#) [Title Only](#) [Author and Title](#)

Hosmani, P. S., Flores-Gonzalez, M., van de Geest, H., Maumus, F., Bakker, L. v., Schijlen, E., van Haarst, J., Cordewener, J., Sanchez-Perez, G., Peters, S., Fei, Z., Giovannoni, J. J., Mueller, L. A., & Saha, S. (2019). An improved *de novo* assembly and annotation of the tomato reference genome using single-molecule sequencing, Hi-C proximity ligation and optical maps. *BioRxiv*, 767764. <https://doi.org/10.1101/767764>

Google Scholar: [Author Only](#) [Title Only](#) [Author and Title](#)

Hu, J.-Y., & Saedler, H. (2007). Evolution of the Inflated Calyx Syndrome in Solanaceae. *Molecular Biology and Evolution*, 24(11), 2443–2453. <https://doi.org/10.1093/molbev/msm177>

Google Scholar: [Author Only](#) [Title Only](#) [Author and Title](#)

Huang, M., He, J.-X., Hu, H.-X., Zhang, K., Wang, X.-N., Zhao, B.-B., Lou, H.-X., Ren, D.-M., & Shen, T. (2020). Withanolides from the genus *Physalis*: a review on their phytochemical and pharmacological aspects. *Journal of Pharmacy and Pharmacology*, 72(5), 649–669. <https://doi.org/10.1111/jphp.13209>

Google Scholar: [Author Only](#) [Title Only](#) [Author and Title](#)

Itkin, M., Seybold, H., Breitel, D., Rogachev, I., Meir, S., & Aharoni, A. (2009). TOMATO AGAMOUS-LIKE 1 is a component of the fruit ripening regulatory network. *The Plant Journal*, 60(6), 1081–1095. <https://doi.org/https://doi.org/10.1111/j.1365-313X.2009.04064.x>

Google Scholar: [Author Only](#) [Title Only](#) [Author and Title](#)

Jain, C., Rhie, A., Hansen, N., Koren, S., & Phillippy, A. M. (2020). A long read mapping method for highly repetitive reference sequences. *BioRxiv*, 2020.11.01.363887. <https://doi.org/10.1101/2020.11.01.363887>

Google Scholar: [Author Only](#) [Title Only](#) [Author and Title](#)

Jain, C., Rhie, A., Zhang, H., Chu, C., Walenz, B. P., Koren, S., & Phillippy, A. M. (2020). Weighted minimizer sampling improves long read mapping. *Bioinformatics*, 36(Supplement_1), i111–i118. <https://doi.org/10.1093/bioinformatics/btaa435>

Google Scholar: [Author Only](#) [Title Only](#) [Author and Title](#)

Katoh, K., & Standley, D. M. (2013). MAFFT Multiple Sequence Alignment Software Version 7: Improvements in Performance and Usability. *Molecular Biology and Evolution*, 30(4), 772–780. <https://doi.org/10.1093/molbev/mst010>

Google Scholar: [Author Only](#) [Title Only](#) [Author and Title](#)

Kim, S., Park, M., Yeom, S.-I., Kim, Y.-M., Lee, J. M., Lee, H.-A., Seo, E., Choi, J., Cheong, K., Kim, K.-T., Jung, K., Lee, G.-W., Oh, S.-K., Bae, C., Kim, S.-B., Lee, H.-Y., Kim, S.-Y., Kim, M.-S., Kang, B.-C., ... Choi, D. (2014). Genome sequence of the hot pepper provides insights into the evolution of pungency in *Capsicum* species. *Nature Genetics*, 46(3), 270–278. <https://doi.org/10.1038/ng.2877>

Google Scholar: [Author Only](#) [Title Only](#) [Author and Title](#)

Kirsche, M., Prabhu, G., Sherman, R., Ni, B., Aganezov, S., & Schatz, M. C. (2021). Jasmine: Population-scale structural variant comparison and analysis. *BioRxiv*, 2021.05.27.445886. <https://doi.org/10.1101/2021.05.27.445886>

Google Scholar: [Author Only](#) [Title Only](#) [Author and Title](#)

Kolmogorov, M., Yuan, J., Lin, Y., & Pevzner, P. A. (2019). Assembly of long, error-prone reads using repeat graphs. *Nature Biotechnology*, 37(5), 540–546. <https://doi.org/10.1038/s41587-019-0072-8>

Google Scholar: [Author Only](#) [Title Only](#) [Author and Title](#)

Kurtz, S., Phillippy, A., Delcher, A. L., Smoot, M., Shumway, M., Antonescu, C., & Salzberg, S. L. (2004). Versatile and open software for comparing large genomes. *Genome Biology*, 5(2), R12. <https://doi.org/10.1186/gb-2004-5-2-r12>

Google Scholar: [Author Only](#) [Title Only](#) [Author and Title](#)

Kwon, C.-T., Tang, L., Wang, X., Gentile, I., Hendelman, A., Robitaille, G., Van Eck, J., Xu, C., & Lippman, Z. B. (2022). Dynamic evolution of small signalling peptide compensation in plant stem cell control. *Nature Plants*, 8(4), 346–355. <https://doi.org/10.1038/s41477-022-01118-w>

Google Scholar: [Author Only](#) [Title Only](#) [Author and Title](#)

Lemmon, Z. H., Reem, N. T., Dalrymple, J., Soyk, S., Swartwood, K. E., Rodriguez-Leal, D., van Eck, J., & Lippman, Z. B. (2018). Rapid improvement of domestication traits in an orphan crop by genome editing. *Nature Plants*, 4(10), 766–770. <https://doi.org/10.1038/s41477-018-0259-x>

Google Scholar: [Author Only](#) [Title Only](#) [Author and Title](#)

Li, H. (2013). Aligning sequence reads, clone sequences and assembly contigs with BWA-MEM. *ArXiv: Genomics*.

Google Scholar: [Author Only](#) [Title Only](#) [Author and Title](#)

Li, H. (2018). Minimap2: pairwise alignment for nucleotide sequences. *Bioinformatics*, 34(18), 3094–3100. <https://doi.org/10.1093/bioinformatics/bty191>

Google Scholar: [Author Only](#) [Title Only](#) [Author and Title](#)

Li, H., Handsaker, B., Wysoker, A., Fennell, T., Ruan, J., Homer, N., Marth, G., Abecasis, G., Durbin, R., & Subgroup, 1000 Genome Project Data Processing. (2009). The Sequence Alignment/Map format and SAMtools. *Bioinformatics*, 25(16), 2078–2079. <https://doi.org/10.1093/bioinformatics/btp352>

Google Scholar: [Author Only](#) [Title Only](#) [Author and Title](#)

Li, J., Song, C., & He, C. (2019). Chinese lantern in *Physalis* is an advantageous morphological novelty and improves plant fitness. *Scientific Reports*, 9(1), 596. <https://doi.org/10.1038/s41598-018-36436-7>

Google Scholar: [Author Only](#) [Title Only](#) [Author and Title](#)

Liu, Y., Tikunov, Y., Schouten, R. E., Marcelis, L. F. M., Visser, R. G. F., & Bovy, A. (2018). Anthocyanin Biosynthesis and Degradation Mechanisms in Solanaceous Vegetables: A Review. *Frontiers in Chemistry*, 6. <https://www.frontiersin.org/articles/10.3389/fchem.2018.00052>

Google Scholar: [Author Only](#) [Title Only](#) [Author and Title](#)

Love, M. I., Huber, W., & Anders, S. (2014). Moderated estimation of fold change and dispersion for RNA-seq data with DESeq2. *Genome Biology*, 15(12), 550. <https://doi.org/10.1186/s13059-014-0550-8>

Google Scholar: [Author Only](#) [Title Only](#) [Author and Title](#)

Lu, J., Luo, M., Wang, L., Li, K., Yu, Y., Yang, W., Gong, P., Gao, H., Li, Q., Zhao, J., Wu, L., Zhang, M., Liu, X., Zhang, X., Kang, J., Yu, T., Li, Z., Jiao, Y., ... He, C. (2021). The *Physalis floridana* genome provides insights into the biochemical and morphological evolution of *Physalis* fruits. *Horticulture Research*, 8(1), 244. <https://doi.org/10.1038/s41438-021-00705-w>

Google Scholar: [Author Only](#) [Title Only](#) [Author and Title](#)

Mapleson, D., Venturini, L., Kaithakottil, G., & Swarbreck, D. (2018). Efficient and accurate detection of splice junctions from RNA-seq with Portcullis. *GigaScience*, 7(12), giy131. <https://doi.org/10.1093/gigascience/giy131>

Google Scholar: [Author Only](#) [Title Only](#) [Author and Title](#)

Marini, F., & Binder, H. (2019). pcaExplorer: an R/Bioconductor package for interacting with RNA-seq principal components. *BMC Bioinformatics*, 20(1), 331. <https://doi.org/10.1186/s12859-019-2879-1>

Google Scholar: [Author Only](#) [Title Only](#) [Author and Title](#)

Martínez, M. (1993). The correct application of *Physalis pruinosa* L. (Solanaceae). *TAXON*, 42(1), 103–104. <https://doi.org/https://doi.org/10.2307/1223312>

Google Scholar: [Author Only](#) [Title Only](#) [Author and Title](#)

Meir, Z., Aviezer, I., Chongloi, G. L., Ben-Kiki, O., Bronstein, R., Mukamel, Z., Keren-Shaul, H., Jaitin, D., Tal, L., Shalev-Schlosser, G., Harel, T. H., Tanay, A., & Eshed, Y. (2021). Dissection of floral transition by single-meristem transcriptomes at high temporal resolution. *Nature Plants*, 7(6), 800–813. <https://doi.org/10.1038/s41477-021-00936-8>

Google Scholar: [Author Only](#) [Title Only](#) [Author and Title](#)

Minh, B. Q., Schmidt, H. A., Chernomor, O., Schrempf, D., Woodhams, M. D., von Haeseler, A., & Lanfear, R. (2020). IQ-TREE 2: New Models and Efficient Methods for Phylogenetic Inference in the Genomic Era. *Molecular Biology and Evolution*, 37(5), 1530–1534. <https://doi.org/10.1093/molbev/msaa015>

Google Scholar: [Author Only](#) [Title Only](#) [Author and Title](#)

Morel, P., Heijmans, K., Rozier, F., Zethof, J., Chamot, S., Bento, S. R., Viallette-Guiraud, A., Chambrier, P., Trehin, C., & Vandenbussche, M. (2017). Divergence of the Floral A-Function between an Asterid and a Rosid Species. *The Plant Cell*, 29(7), 1605–1621. <https://doi.org/10.1105/tpc.17.00098>

Google Scholar: [Author Only](#) [Title Only](#) [Author and Title](#)

Morgulis, A., Gertz, E. M., Schäffer, A. A., & Agarwala, R. (2006). WindowMasker: window-based masker for sequenced genomes. *Bioinformatics*, 22(2), 134–141. <https://doi.org/10.1093/bioinformatics/bti774>

Google Scholar: [Author Only](#) [Title Only](#) [Author and Title](#)

Muller, G. B., & Wagner, G. P. (1991). Novelty in Evolution: Restructuring the Concept. *Annual Review of Ecology and Systematics*, 22, 229–256. <http://www.jstor.org/stable/2097261>

Google Scholar: [Author Only](#) [Title Only](#) [Author and Title](#)

Nurk, S., Walenz, B. P., Rhie, A., Vollger, M. R., Logsdon, G. A., Grothe, R., Miga, K. H., Eichler, E. E., Phillippy, A. M., & Koren, S. (2020). HiCanu: accurate assembly of segmental duplications, satellites, and allelic variants from high-fidelity long reads. *Genome Research*, 30(9), 1291–1305. <https://doi.org/10.1101/gr.263566.120>

Google Scholar: [Author Only](#) [Title Only](#) [Author and Title](#)

Ou, S., Su, W., Liao, Y., Chougule, K., Agda, J. R. A., Hellinga, A. J., Lugo, C. S. B., Elliott, T. A., Ware, D., Peterson, T., Jiang, N., Hirsch, C. N., & Hufford, M. B. (2019). Benchmarking transposable element annotation methods for creation of a streamlined, comprehensive pipeline. *Genome Biology*, 20(1), 275. <https://doi.org/10.1186/s13059-019-1905-y>

Google Scholar: [Author Only](#) [Title Only](#) [Author and Title](#)

Padmaja, H., Sruthi, S. R., & Vangalapati, M. (2014). INTERNATIONAL JOURNAL OF PHARMACY & LIFE SCIENCES (Int. J. of Pharm. Life Sci.) Review on Hibiscus sabdariffa - A valuable herb.

Google Scholar: [Author Only](#) [Title Only](#) [Author and Title](#)

Pan, I. L., McQuinn, R., Giovannoni, J. J., & Irish, V. F. (2010). Functional diversification of AGAMOUS lineage genes in regulating tomato flower and fruit development. *Journal of Experimental Botany*, 61(6), 1795–1806. <https://doi.org/10.1093/jxb/erq046>

Google Scholar: [Author Only](#) [Title Only](#) [Author and Title](#)

Park, S. J., Eshed, Y., & Lippman, Z. B. (2014). Meristem maturation and inflorescence architecture-lessons from the Solanaceae. *Current Opinion in Plant Biology*, 17, 70–77. <https://doi.org/https://doi.org/10.1016/j.pbi.2013.11.006>

Google Scholar: [Author Only](#) [Title Only](#) [Author and Title](#)

Paton, A. (1990). A Global Taxonomic Investigation of *Scutellaria* (Labiateae). *Kew Bulletin*, 45(3), 399–450. <https://doi.org/10.2307/4110512>

Google Scholar: [Author Only](#) [Title Only](#) [Author and Title](#)

Patro, R., Duggal, G., Love, M. I., Irizarry, R. A., & Kingsford, C. (2017). Salmon provides fast and bias-aware quantification of transcript expression. *Nature Methods*, 14(4), 417–419. <https://doi.org/10.1038/nmeth.4197>

Google Scholar: [Author Only](#) [Title Only](#) [Author and Title](#)

Pertea, G., & Pertea, M. (2020). GFF Utilities: GffRead and GffCompare [version 2; peer review: 3 approved] . *F1000Research*, 9(304). <https://doi.org/10.12688/f1000research.23297.2>

Google Scholar: [Author Only](#) [Title Only](#) [Author and Title](#)

Pertea, M., Pertea, G. M., Antonescu, C. M., Chang, T.-C., Mendell, J. T., & Salzberg, S. L. (2015). StringTie enables improved reconstruction of a transcriptome from RNA-seq reads. *Nature Biotechnology*, 33(3), 290–295. <https://doi.org/10.1038/nbt.3122>

Google Scholar: [Author Only](#) [Title Only](#) [Author and Title](#)

Picard toolkit. (2019). In Broad Institute, GitHub repository. Broad Institute.

Google Scholar: [Author Only](#) [Title Only](#) [Author and Title](#)

Pnueli, L., Hareven, D., Rounsley, S. D., Yanofsky, M. F., & Lifschitz, E. (1994). Isolation of the Tomato AGAMOUS Gene TAG1 and Analysis of Its Homeotic Role in Transgenic Plants. *The Plant Cell*, 6(2), 163–173. <https://doi.org/10.2307/3869636>

Google Scholar: [Author Only](#) [Title Only](#) [Author and Title](#)

Pretz, C., & Deanna, R. (2020). Typifications and nomenclatural notes in *Physalis* (Solanaceae) from the United States. *TAXON*, 69(1), 170–192. <https://doi.org/https://doi.org/10.1002/tax.12159>

Google Scholar: [Author Only](#) [Title Only](#) [Author and Title](#)

R Core Team. (2020). R: A Language and Environment for Statistical Computing. <https://www.R-project.org/>

Google Scholar: [Author Only](#) [Title Only](#) [Author and Title](#)

Rhie, A., McCarthy, S. A., Fedrigo, O., Damas, J., Formenti, G., Koren, S., Uliano-Silva, M., Chow, W., Fungtammasan, A., Kim, J., Lee, C., Ko, B. J., Chaisson, M., Gedman, G. L., Cantin, L. J., Thibaud-Nissen, F., Haggerty, L., Bista, I., Smith, M., ... Jarvis, E. D. (2021). Towards complete and error-free genome assemblies of all vertebrate species. *Nature*, 592(7856), 737–746. <https://doi.org/10.1038/s41586-021-03451-0>

Google Scholar: [Author Only](#) [Title Only](#) [Author and Title](#)

Rhie, A., Walenz, B. P., Koren, S., & Phillippy, A. M. (2020). Merquy: reference-free quality, completeness, and phasing assessment for genome assemblies. *Genome Biology*, 21(1), 245. <https://doi.org/10.1186/s13059-020-02134-9>

Google Scholar: [Author Only](#) [Title Only](#) [Author and Title](#)

Rydberg, P. A. (1896). The North American species of *Physalis* and related genera. New York: Torrey Botanical Club.

Google Scholar: [Author Only](#) [Title Only](#) [Author and Title](#)

Särkinen, T., Bohs, L., Olmstead, R. G., & Knapp, S. (2013). A phylogenetic framework for evolutionary study of the nightshades (Solanaceae): a dated 1000-tip tree. *BMC Evolutionary Biology*, 13(1), 214. <https://doi.org/10.1186/1471-2148-13-214>

Google Scholar: [Author Only](#) [Title Only](#) [Author and Title](#)

Sato, S., Tabata, S., Hirakawa, H., Asamizu, E., Shirasawa, K., Isobe, S., Kaneko, T., Nakamura, Y., Shibata, D., Aoki, K., Egholm, M., Knight, J., Bogden, R., Li, C., Shuang, Y., Xu, X., Pan, S., Cheng, S., Liu, X., ... Fabra, U. P. (2012). The tomato genome sequence provides insights into fleshy fruit evolution. *Nature*, 485(7400), 635–641. <https://doi.org/10.1038/nature11119>

Google Scholar: [Author Only](#) [Title Only](#) [Author and Title](#)

Senthil-Kumar, M., & Mysore, K. S. (2011). Caveat of RNAi in Plants: The Off-Target Effect. In H. Kodama & A. Komamine (Eds.), *RNAi and Plant Gene Function Analysis: Methods and Protocols* (pp. 13–25). Humana Press. https://doi.org/10.1007/978-1-61779-123-9_2

Google Scholar: [Author Only](#) [Title Only](#) [Author and Title](#)

Shenstone, E., Lippman, Z., & van Eck, J. (2020). A review of nutritional properties and health benefits of *Physalis* species. *Plant Foods for Human Nutrition*, 75(3), 316–325. <https://doi.org/10.1007/s11130-020-00821-3>

Google Scholar: [Author Only](#) [Title Only](#) [Author and Title](#)

Shubin, N., Tabin, C., & Carroll, S. (2009). Deep homology and the origins of evolutionary novelty. *Nature*, 457(7231), 818–823. <https://doi.org/10.1038/nature07891>

Google Scholar: [Author Only](#) [Title Only](#) [Author and Title](#)

Shumate, A., & Salzberg, S. L. (2021). Liftoff: accurate mapping of gene annotations. *Bioinformatics*, 37(12), 1639–1643. <https://doi.org/10.1093/bioinformatics/btaa1016>

Google Scholar: [Author Only](#) [Title Only](#) [Author and Title](#)

Simão, F. A., Waterhouse, R. M., Ioannidis, P., Kriventseva, E. v., & Zdobnov, E. M. (2015). BUSCO: assessing genome assembly and annotation completeness with single-copy orthologs. *Bioinformatics*, 31(19), 3210–3212. <https://doi.org/10.1093/bioinformatics/btv351>

Google Scholar: [Author Only](#) [Title Only](#) [Author and Title](#)

- Soneson, C., Love, M. I., & Robinson, M. D. (2016). Differential analyses for RNA-seq: transcript-level estimates improve gene-level inferences [version 2; peer review: 2 approved] . F1000Research, 4(1521). <https://doi.org/10.12688/f1000research.7563.2>
Google Scholar: [Author Only](#) [Title Only](#) [Author and Title](#)
- Soyk, S., Lemmon, Z. H., Oved, M., Fisher, J., Liberatore, K. L., Park, S. J., Goren, A., Jiang, K., Ramos, A., van der Knaap, E., van Eck, J., Zamir, D., Eshed, Y., & Lippman, Z. B. (2017). Bypassing Negative Epistasis on Yield in Tomato Imposed by a Domestication Gene. *Cell*, 169(6), 1142-1155.e12. <https://doi.org/10.1016/j.cell.2017.04.032>
Google Scholar: [Author Only](#) [Title Only](#) [Author and Title](#)
- Spelt, C., Quattrocchio, F., Mol, J., & Koes, R. (2002). ANTHOCYANIN1 of Petunia Controls Pigment Synthesis, Vacuolar pH, and Seed Coat Development by Genetically Distinct Mechanisms. *The Plant Cell*, 14(9), 2121–2135. <https://doi.org/10.1105/tpc.003772>
Google Scholar: [Author Only](#) [Title Only](#) [Author and Title](#)
- Spelt, C., Quattrocchio, F., Mol, J. N. M., & Koes, R. (2000). anthocyanin1 of Petunia Encodes a Basic Helix-Loop-Helix Protein That Directly Activates Transcription of Structural Anthocyanin Genes. *The Plant Cell*, 12(9), 1619–1631. <https://doi.org/10.1105/tpc.12.9.1619>
Google Scholar: [Author Only](#) [Title Only](#) [Author and Title](#)
- Sugiyama, Y., Watase, Y., Nagase, M., Makita, N., Yagura, S., Hirai, A., & Sugiura, M. (2005). The complete nucleotide sequence and multipartite organization of the tobacco mitochondrial genome: comparative analysis of mitochondrial genomes in higher plants. *Molecular Genetics and Genomics*, 272(6), 603–615. <https://doi.org/10.1007/s00438-004-1075-8>
Google Scholar: [Author Only](#) [Title Only](#) [Author and Title](#)
- Swartwood, K., & van Eck, J. (2019). Development of plant regeneration and *Agrobacterium tumefaciens*-mediated transformation methodology for *Physalis pruinosa*. *Plant Cell, Tissue and Organ Culture (PCTOC)*, 137(3), 465–472. <https://doi.org/10.1007/s11240-019-01582-x>
Google Scholar: [Author Only](#) [Title Only](#) [Author and Title](#)
- Takagi, H., Abe, A., Yoshida, K., Kosugi, S., Natsume, S., Mitsuoka, C., Uemura, A., Utsushi, H., Tamiru, M., Takuno, S., Innan, H., Cano, L. M., Kamoun, S., & Terauchi, R. (2013). QTL-seq: rapid mapping of quantitative trait loci in rice by whole genome resequencing of DNA from two bulked populations. *The Plant Journal*, 74(1), 174–183. <https://doi.org/https://doi.org/10.1111/tpj.12105>
Google Scholar: [Author Only](#) [Title Only](#) [Author and Title](#)
- Tamura, K., Stecher, G., & Kumar, S. (2021). MEGA11: Molecular Evolutionary Genetics Analysis Version 11. *Molecular Biology and Evolution*, 38(7), 3022–3027. <https://doi.org/10.1093/molbev/msab120>
Google Scholar: [Author Only](#) [Title Only](#) [Author and Title](#)
- Theißen, G., & Saedler, H. (2001). Floral quartets. *Nature*, 409(6819), 469–471. <https://doi.org/10.1038/35054172>
Google Scholar: [Author Only](#) [Title Only](#) [Author and Title](#)
- Venturini, L., Caim, S., Kaithakottil, G. G., Mapleson, D. L., & Swarbreck, D. (2018). Leveraging multiple transcriptome assembly methods for improved gene structure annotation. *GigaScience*, 7(8), giy093. <https://doi.org/10.1093/gigascience/giy093>
Google Scholar: [Author Only](#) [Title Only](#) [Author and Title](#)
- Waterfall, U. T. (1967). PHYSALIS IN MEXICO, CENTRAL AMERICA AND THE WEST INDIES. *Rhodora*, 69(777), 82–120. <http://www.jstor.org/stable/23311644>
Google Scholar: [Author Only](#) [Title Only](#) [Author and Title](#)
- Waterfall, U. T. (Urnaldy T. (1958). A taxonomic study of the genus *Physalis* in North America north of Mexico. *Rhodora*, 60, 152–173. <https://www.biodiversitylibrary.org/part/124500>
Google Scholar: [Author Only](#) [Title Only](#) [Author and Title](#)
- Wei, Q., Wang, J., Wang, W., Hu, T., Hu, H., & Bao, C. (2020). A high-quality chromosome-level genome assembly reveals genetics for important traits in eggplant. *Horticulture Research*, 7(1), 153. <https://doi.org/10.1038/s41438-020-00391-0>
Google Scholar: [Author Only](#) [Title Only](#) [Author and Title](#)
- Weigel, D., & Meyerowitz, E. M. (1994). The ABCs of floral homeotic genes. *Cell*, 78(2), 203–209. [https://doi.org/https://doi.org/10.1016/0092-8674\(94\)90291-7](https://doi.org/https://doi.org/10.1016/0092-8674(94)90291-7)
Google Scholar: [Author Only](#) [Title Only](#) [Author and Title](#)
- Whitson, M. (2012). CALLIPHYSALIS (SOLANACEAE): A NEW GENUS FROM THE SOUTHEASTERN USA *Rhodora*, 114(958), 133–147. <http://www.jstor.org/stable/23314732>
Google Scholar: [Author Only](#) [Title Only](#) [Author and Title](#)
- Wilf, P., Carvalho, M. R., Gandolfo, M. A., & Cúneo, N. R. (2017). Eocene lantern fruits from Gondwanan Patagonia and the early origins of Solanaceae. *Science*, 355(6320), 71–75. <https://doi.org/10.1126/science.aag2737>
Google Scholar: [Author Only](#) [Title Only](#) [Author and Title](#)
- Xu, P., Zhang, Y., Kang, L., Roossinck, M. J., & Mysore, K. S. (2006). Computational Estimation and Experimental Verification of

Off-Target Silencing during Posttranscriptional Gene Silencing in Plants. *Plant Physiology*, 142(2), 429–440.
<https://doi.org/10.1104/pp.106.083295>

Google Scholar: [Author Only](#) [Title Only](#) [Author and Title](#)

Xu, X., Pan, S., Cheng, S., Zhang, B., Mu, D., Ni, P., Zhang, G., Yang, S., Li, R., Wang, J., Orjeda, G., Guzman, F., Torres, M., Lozano, R., Ponce, O., Martinez, D., de la Cruz, G., Chakrabarti, S. K., Patil, V. U., ... Centre, W. U. & R. (2011). Genome sequence and analysis of the tuber crop potato. *Nature*, 475(7355), 189–195. <https://doi.org/10.1038/nature10158>

Google Scholar: [Author Only](#) [Title Only](#) [Author and Title](#)

Yanofsky, M. F., Ma, H., Bowman, J. L., Drews, G. N., Feldmann, K. A., & Meyerowitz, E. M. (1990). The protein encoded by the *Arabidopsis* homeotic gene *agamous* resembles transcription factors. *Nature*, 346(6279), 35–39. <https://doi.org/10.1038/346035a0>

Google Scholar: [Author Only](#) [Title Only](#) [Author and Title](#)

Yuste-Lisbona, F. J., Quinet, M., Fernández-Lozano, A., Pineda, B., Moreno, V., Angosto, T., & Lozano, R. (2016). Characterization of vegetative inflorescence (*mc-vin*) mutant provides new insight into the role of *MACROCALYX* in regulating inflorescence development of tomato. *Scientific Reports*, 6(1), 18796. <https://doi.org/10.1038/srep18796>

Google Scholar: [Author Only](#) [Title Only](#) [Author and Title](#)

Zamora-Tavares, M. del P., Martínez, M., Magallón, S., Guzmán-Dávalos, L., & Vargas-Ponce, O. (2016). *Physalis* and physaloids: A recent and complex evolutionary history. *Molecular Phylogenetics and Evolution*, 100, 41–50.
<https://doi.org/https://doi.org/10.1016/j.ympev.2016.03.032>

Google Scholar: [Author Only](#) [Title Only](#) [Author and Title](#)

Zhang, J.-S., Li, Z., Zhao, J., Zhang, S., Quan, H., Zhao, M., & He, C. (2014). Deciphering the *Physalis floridana* Double-Layered-Lantern1 Mutant Provides Insights into Functional Divergence of the *GLOBOSA* Duplicates within the Solanaceae . *Plant Physiology*, 164(2), 748–764. <https://doi.org/10.1104/pp.113.233072>

Google Scholar: [Author Only](#) [Title Only](#) [Author and Title](#)

Zhang, W.-N., & Tong, W.-Y. (2016). Chemical Constituents and Biological Activities of Plants from the Genus *Physalis*. *Chemistry & Biodiversity*, 13(1), 48–65. <https://doi.org/https://doi.org/10.1002/cbdv.201400435>

Google Scholar: [Author Only](#) [Title Only](#) [Author and Title](#)

Zhao, J., Tian, Y., Zhang, J.-S., Zhao, M., Gong, P., Riss, S., Saedler, R., & He, C. (2013). The euAP1 protein MPF3 represses MPF2 to specify floral calyx identity and displays crucial roles in Chinese lantern development in *Physalis*. *The Plant Cell*, 25(6), 2002–2021. <https://doi.org/10.1105/tpc.113.111757>

Google Scholar: [Author Only](#) [Title Only](#) [Author and Title](#)